Article

Neuron

An Intrinsic Epigenetic Barrier for Functional Axon Regeneration

Highlights

- Peripheral nerve lesion elevates Tet3 and 5hmC levels in mature DRG neurons
- Tet3 is required for axon regeneration of DRG neurons and behavioral recovery
- TET3 and TDG mediate injury-induced DNA demethylation and expression of RAGs
- TET1 is required for PETN-deletion-induced axonal regeneration of mature RGCs

Authors

Yi-Lan Weng, Ran An, Jessica Cassin, ..., Zhigang He, Hongjun Song, Guo-li Ming

Correspondence

shongjun@mail.med.upenn.edu

In Brief

Mature mammalian neurons exhibit little axonal growth. Weng et al. uncovered an epigenetic mechanism wherein axonal injury elevates the active DNA demethylation pathway to induce regeneration-associated gene expression, which in turn promotes functional axonal regeneration of peripheral sensory neurons.

Weng et al., 2017, Neuron *94*, 337–346
April 19, 2017
http://dx.doi.org/10.1016/j.neuron.2017.03.034

CellPress

Neuron
Article

An Intrinsic Epigenetic Barrier for Functional Axon Regeneration

Yi-Lan Weng,[1,2,12] Ran An,[1,2,3,12] Jessica Cassin,[1,4,12] Jessica Joseph,[1,5] Ruifa Mi,[2] Chen Wang,[6] Chun Zhong,[1,2] Seung-Gi Jin,[7] Gerd P. Pfeifer,[7] Alfonso Bellacosa,[8] Xinzhong Dong,[9] Ahmet Hoke,[2] Zhigang He,[6] Hongjun Song,[1,2,4,5,9,10,13,14,*] and Guo-li Ming[1,2,5,9,10,11,13]

[1]Institute for Cell Engineering
[2]Department of Neurology
Johns Hopkins University School of Medicine, Baltimore, MD 21205, USA
[3]Department of Neurology, Huashan Hospital, State Key Laboratory of Medical Neurobiology, Fudan University, Shanghai 200040, China
[4]Pre-doctoral Human Genetics Training Program
[5]Graduate Program in Cellular and Molecular Medicine
Johns Hopkins University School of Medicine, Baltimore, MD 21205, USA
[6]F.M. Kirby Neurobiology Center and Department of Neurology, Boston Children's Hospital, 300 Longwood Avenue, Boston, MA 02115, USA
[7]Center for Epigenetics, Van Andel Research Institute, Grand Rapids, MI 49503, USA
[8]Cancer Epigenetics and Cancer Biology Programs, Fox Chase Cancer Center, Philadelphia, PA 19111, USA
[9]The Solomon H. Snyder Department of Neuroscience, Johns Hopkins University School of Medicine, Baltimore, MD 21205, USA
[10]Department of Neuroscience, Mahoney Institute for Neurosciences, Perelman School for Medicine, University of Pennsylvania, Philadelphia, PA 19104, USA
[11]Department of Psychiatry and Behavioral Sciences, Johns Hopkins University School of Medicine, Baltimore, MD 21205, USA
[12]These authors contributed equally
[13]Senior author
[14]Lead Contact
*Correspondence: shongjun@mail.med.upenn.edu
http://dx.doi.org/10.1016/j.neuron.2017.03.034

SUMMARY

Mature neurons in the adult peripheral nervous system can effectively switch from a dormant state with little axonal growth to robust axon regeneration upon injury. The mechanisms by which injury unlocks mature neurons' intrinsic axonal growth competence are not well understood. Here, we show that peripheral sciatic nerve lesion in adult mice leads to elevated levels of Tet3 and 5-hydroxylmethylcytosine in dorsal root ganglion (DRG) neurons. Functionally, Tet3 is required for robust axon regeneration of DRG neurons and behavioral recovery. Mechanistically, peripheral nerve injury induces DNA demethylation and upregulation of multiple regeneration-associated genes in a Tet3- and thymine DNA glycosylase-dependent fashion in DRG neurons. In addition, Pten deletion-induced axon regeneration of retinal ganglion neurons in the adult CNS is attenuated upon Tet1 knockdown. Together, our study suggests an epigenetic barrier that can be removed by active DNA demethylation to permit axon regeneration in the adult mammalian nervous system.

INTRODUCTION

Epigenetic DNA methylation marks are established during development and function as a basic mechanism to maintain stable cellular states via the silencing of gene expression upon terminal differentiation (Jaenisch and Bird, 2003; Ma et al., 2010). Unlike developing neurons with robust growth capacity, mature mammalian neurons enter into a dormant growth state and maintain an intrinsic barrier to extensive axonal growth in the adult peripheral nervous system (PNS) and central nervous system (CNS) (Goldberg et al., 2002; He and Jin, 2016; Liu et al., 2011; Rossi et al., 2007; Zhou and Snider, 2006). Interestingly, peripheral axon injuries switch adult dorsal root ganglion (DRG) neurons to a pro-regenerative state via de novo gene transcription (Costigan et al., 2002; Moore and Goldberg, 2011; Smith and Skene, 1997). In the adult CNS, axon regeneration can also be induced, for example by deletion of PTEN in retinal ganglion neurons and corticospinal neurons (Liu et al., 2010; Park et al., 2008). Previous studies have mostly focused on cytoplasmic signaling and transcription factor-based mechanisms to promote intrinsic axon growth capacity, mostly with manipulations of one or two genes at a time (Hammarlund and Jin, 2014; Liu et al., 2011; Moore and Goldberg, 2011; Tedeschi and Bradke, 2017). Given that global and sustained gene induction is necessary for regenerative axonal growth to occur in injured neurons, epigenetic mechanisms could play a pivotal role in providing transcription factors access to developmentally silenced genomic loci and in orchestrating transcriptional reactivation of a large repertoire of regeneration-associated genes (RAGs) (Cho and Cavalli, 2014; Trakhtenberg and Goldberg, 2012; Weng et al., 2016; Wong and Zou, 2014). Indeed, histone modifications, which are essential for the maintenance of barriers between transcriptionally active euchromatin and transcriptionally silent heterochromatin, have previously been implicated in PNS axon regeneration (Cho et al., 2013; Finelli et al., 2013; Gaub et al., 2011; Puttagunta et al., 2014). Notably, regulation of histone acetylation

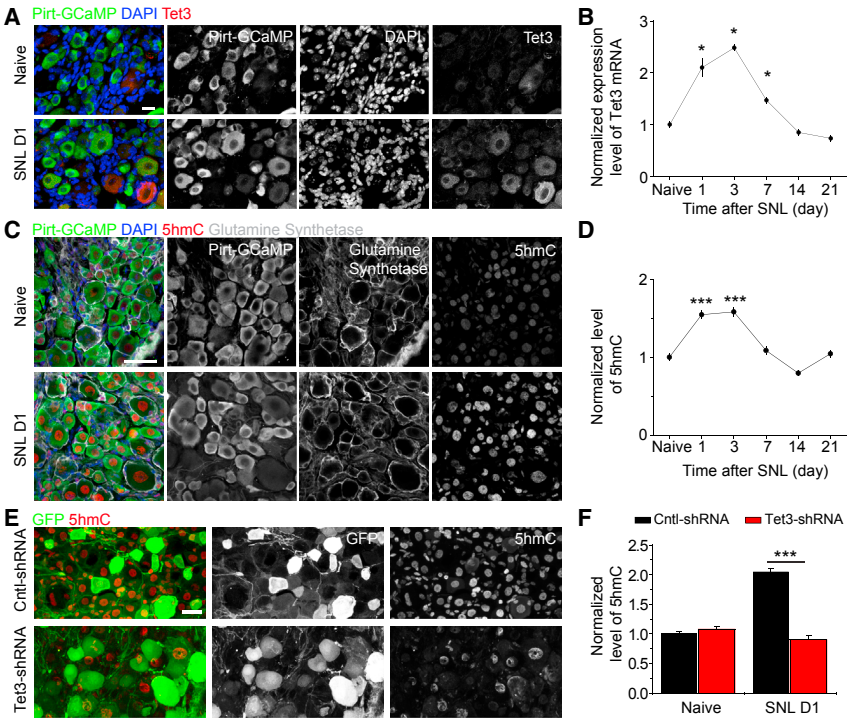

Figure 1. SNL Upregulates Tet3 and 5hmC Levels in Adult DRG Neurons In Vivo

(A) Sample confocal images of Tet3 in situ, GFP immunostaining, and DAPI of L4 DRGs in adult Pirt-GCaMP3 neuronal reporter mice under naive conditions and at 1 day upon sciatic nerve lesion (SNL). Scale bar, 20 μm.

(B) Time course of Tet3 induction in axotomized DRGs by qPCR analysis. Values represent mean ± SEM (n = 3 for each group; *p < 0.05; two-way ANOVA).

(C) Sample confocal image of immunostaining for GFP, 5hmC, glutamine synthetase, a marker for glia, and DAPI in DRGs of adult Pirt-GCaMP3 neuronal reporter mice under naive conditions and at SNL D1. Scale bar, 50 μm.

(D) Quantification of 5hmC levels at different time points after SNL. The signal intensity in NeuN$^+$ neuronal nuclei of naive L4 DRGs was set as 1.0 and 100–180 neuronal nuclei from each condition in three independent experiments were quantified. Values represent mean ± SEM (n = 3 for each group; ***p < 0.001; two-way ANOVA).

(E and F) Immunohistochemical analysis of 5hmC levels in Ctrl and Tet3 KD DRG neurons under naive conditions and at SNL D1. Shown are sample images (E) (scale bar, 20 μm) and quantification (F). Similar to (D). Values represent mean ± SEM (n = 3 for each group; ***p < 0.001; two-way ANOVA).

via HDAC is essential for axon regeneration in the adult PNS but is not sufficient to activate the expression of several well-established RAGs, such as ATF3 and Smad1, therefore suggesting additional barriers (Finelli et al., 2013).

Originally thought to be largely irreversible in fully differentiated cells, DNA methylation in neurons has recently been shown to be dynamically regulated during development and in response to physiological stimuli (Gräff et al., 2011; Guo et al., 2011a; Lister et al., 2013; Shin et al., 2014b; Yao et al., 2016). The reconfiguration of the neuronal methylome results from the orchestration of both DNA methylation and demethylation processes (Guo et al., 2011a). Ten-eleven translocation methylcytosine dioxygenases (Tets) have been found to iteratively oxidize 5-methylcytosine (5mC) to 5-hydroxymethylcytosine (5hmC), 5-formylcytosine (5fC) and 5-carboxycytosine (5caC), allowing cell-cycle-independent removal of DNA methylation (He et al., 2011; Ito et al., 2011; Tahiliani et al., 2009). Subsequent studies have shown that Tet-initiated DNA oxidation is followed by the thymine DNA glycosylase (TDG)-mediated base excision pathway to complete the demethylation process (Bellacosa and Drohat, 2015; Guo et al., 2011c; He et al., 2011; Ito et al., 2011). Tet family members have been shown to be important for many biological processes including activity-regulated neuronal gene expression, synaptic transmission, and scaling, as well as memory formation and extinction (Feng et al., 2015; Kaas et al., 2013; Rudenko et al., 2013; Yu et al., 2015). One very recent study showed increased 5hmC levels upon axotomy of adult DRG neurons (Loh et al., 2017). However, little is known about the function of DNA methylation in axon regeneration (Iskandar et al., 2010; Puttagunta et al., 2014). The identification of active DNA demethylation machinery provides an entry point to test the hypothesis that DNA demethylation serves as a fundamental mechanism to globally reprogram the cellular state of mature mammalian neurons to permit axonal regeneration.

RESULTS

Peripheral Axon Injury of Adult DRG Neurons Induces Elevation of 5hmC Levels

To screen for epigenetic factors that exhibit responsiveness to axonal injury, we first performed qPCR analysis of known DNA demethylation mediators, including Tet1-3, Apobec1-3, Gadd45a, Gadd45b, Gadd45g, and Tdg (Guo et al., 2011b), in adult DRGs of naive mice and upon sciatic nerve lesion (SNL). Consistent with a previous report (Befort et al., 2003), SNL robustly elevated the expression of Gadd45a, a regulator of active DNA demethylation (Ma et al., 2009) on day 1 (D1) (Figure S1A). Interestingly, Tet3 expression, but not Tet1 and Tet2, was also induced (Figure S1A). In situ analysis showed little Tet1 or Tet2 expression in the adult DRG (Figure S1B). Analysis using a mouse reporter line, which expresses GCaMP3 from the endogenous *Pirt* locus and labels 95% of neurons (but not glia) in the adult DRG (Kim et al., 2016), showed Tet3 induction by SNL to be neuron-specific (Figure 1A). We confirmed Tet3 upregulation at the protein level by western blot (Figure S1C). Time course analysis by qPCR showed that Tet3 expression reached its peak at SNL D3 and returned to basal levels by D14 (Figure 1C). Pharmacological experiments revealed that Tet3 induction in the DRG was attenuated by the Ca^{2+} chelator BAPTA-AM and KN93, an inhibitor of CaMKII, but not KN92, an inactive analog (Figure S1D). It is known that Ca^{2+} is propagated from injured axons back to DRG neuronal nuclei (Cho et al., 2013; Rishal

and Fainzilber, 2014), therefore our results suggest a model wherein Tet3 expression is induced by retrograde Ca^{2+} signaling from injured axons.

Consistent with a role of Tet proteins in oxidizing 5mC to its derivatives, 5hmC levels were increased in Pirt-GCaMP3$^+$ DRG neurons at SNL D1 (Figure 1C). Quantitative dot-blot analysis of semi-purified DRG neurons confirmed the global increase of 5hmC levels, suggesting large-scale epigenetic changes after SNL (Figure S1E). Time course analysis showed that 5hmC levels gradually increased until SNL D3 and returned to basal levels by D21 (Figures 1D and S1F).

To investigate the molecular mechanism underlying injury-induced elevation of 5hmC levels, we infected DRGs via targeted intrathecal AAV2/9-GFP injection, which labeled over 70% of all neurons in L4/5 DRGs and their sciatic nerve axons (Figures S1G and S1H). Using previously characterized small hairpin RNA (shRNA) (Yu et al., 2015), we found that induction of 5hmC levels in GFP$^+$ DRG neurons at SNL D1 was abolished upon Tet3 knockdown (KD) (Figures 1E and 1F), suggesting that Tet3 is responsible for the increased 5hmC levels upon SNL.

Tet3 Is Required for Functional Axon Regeneration of Adult DRG Neurons

To examine the potential functional role of Tet3 in injury-induced axonal regeneration, we first used an in vitro neurite outgrowth assay with primary neurons from adult mouse DRGs. Cultures were infected with AAV2/9 to co-express GFP and shRNA against Tet1, Tet2, or Tet3, followed by re-plating to mimic axotomy (Figures S2A and S2B). We found that Tet3 KD, but not Tet1 or Tet2 KD, reduced the number and the total neurite length of neurite-bearing neurons (Figures S2C–S2E).

We next assessed the in vivo role of Tet3 in functional axon regeneration of adult DRG neurons after SNL via intrathecal AAV2/9 injection-mediated expression of GFP and shRNA (Figures S1G and S1H). Regenerating sensory axons were identified by SCG10 immunostaining (Shin et al., 2014c) (Figure 2A). We found that the extension of SCG10$^+$ axons was significantly decreased upon Tet3 KD compared to control animals at SNL D3 (Figure 2B). To validate these results, we directly examined regeneration of GFP$^+$ axons at SNL D7 when pre-existing lesioned axons were fully degenerated (Di Maio et al., 2011; Shin et al., 2012). We quantified the number of regenerating GFP$^+$ axons in coronal sections at incremental distances from the lesion site (Figure S2F). We did not detect any differences in axonal morphology or numbers upon Tet3 KD in the absence of SNL (Figures S2G and S2H). In contrast, there was a significant reduction of axonal growth in Tet3 KD animals at SNL D7 compared to animals injected with control shRNA (Ctrl; Figures 2C and 2D). Notably, over 45% of Tet3 KD neurons failed to extend axons 1 mm or more beyond the lesion site compared to only 17% of Ctrl neurons (Figure 2E). Conversely, over 62% of Ctrl neurons extended axons over 6 mm from the lesion site compared to only 33% of Tet3 KD neurons (Figure 2E). There were few cleaved caspase3$^+$ neurons in the DRG under all conditions (Figure S2I), ruling out the potential contribution of cell death to observed deficits in axon regeneration.

Regenerating axons of sciatic nerves extend to the epidermis and start to re-innervate the skin of the hind paw ~2–3 weeks after injury. Analysis of skin biopsies showed no GFP$^+$ sensory axon innervation to the epidermis of the hind paw at SNL D7, indicating effective degeneration of preexisting mature axons of both Ctrl and Tet3 KD neurons (Figures S2J and S2K). At SNL D21, innervation to all three epidermal zones by GFP$^+$ regenerating axons of Tet3 KD neurons was significantly reduced, but no difference was observed in naive neurons with or without Tet3 KD (Figures 2F and 2G). These results suggest that Tet3 is required for regenerative axonal growth and re-innervation of target areas of the sciatic nerve.

To assess the functional outcome, we performed behavioral tests to quantify the latency of heat-evoked hind paw withdrawal (Wright et al., 2014). Both Ctrl and Tet3 KD animals exhibited similar response latencies to radiant thermal stimulus at SNL D1 and D7 (Figure 2H). Starting from SNL D14, the withdrawal latency gradually recovered in the Ctrl group, but only minimally in Tet3 KD animals (Figure 2H). Together, these results establish that injury-induced Tet3 upregulation plays an essential role in functional sensory axon regeneration of adult DRG neurons.

Tet3 Regulates Expression of Regeneration-Associated Genes

To investigate the molecular mechanism underlying Tet3-dependent axon regeneration, we assessed whether Tet3 regulates the expression of known RAGs. qPCR analysis of DRGs at SNL D1 showed that induction of a subset of RAGs was significantly attenuated by Tet3 KD, including ATF3, Smad1, STAT3, and c-Myc (Costigan et al., 2002; Moore and Goldberg, 2011; Smith and Skene, 1997) (Figure 3A). Interestingly, Tet3 KD also led to decreased expression of some RAGs in naive DRG neurons, including Smad1 and STAT3 (Figure 3A). Thus, Tet3 regulates expression of multiple RAGs both under basal conditions and upon injury.

ATF3 is one of the most robustly induced genes by SNL and has been shown to enhance peripheral nerve regeneration by increasing the intrinsic growth competence of adult DRG neurons (Fagoe et al., 2015; Seijffers et al., 2007). We therefore focused on ATF3 for in-depth analyses. Consistent with a previous finding (Seijffers et al., 2007), ATF3 protein was barely detectable in naive DRGs, but was robustly upregulated at SNL D1 in Pirt-GCaMP3$^+$ DRG neurons and not in glutamine synthetase-expressing glial cells (Figures 3B). Importantly, this induction was greatly attenuated by Tet3 KD (Figures 3C and 3D). The impairment was not due to a delay of ATF3 induction, as the defect persisted through SNL D7 (Figure 3D). Quantitative immunohistological analysis revealed similar levels of phospho-c-Jun in Ctrl and Tet3 KD neurons at SNL D7 (Figures S3A and S3B), suggesting an intact retrograde axonal injury signaling that triggers accumulation of nuclear phospho-c-Jun via the JNK pathway (Rishal and Fainzilber, 2014).

Tet3 Function Is Required for DNA Demethylation of RAGs

To understand how Tet3 regulates the expression of RAGs, we first asked whether SNL induces demethylation of RAGs in adult DRG neurons in vivo. Because the whole DRG contains many times more glial cells than neurons (Delree et al., 1989; Thakur et al., 2014), we enriched neuronal nuclei using a

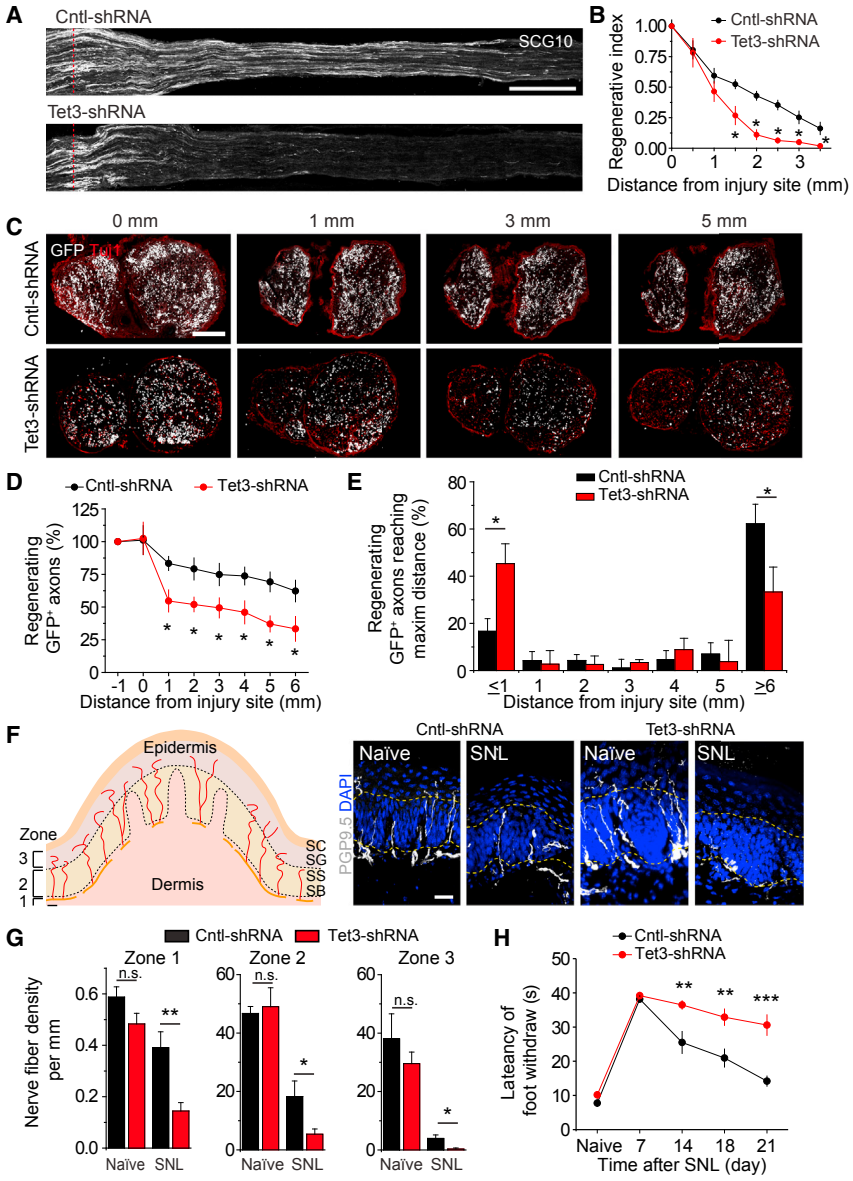

Figure 2. Tet3 Is Required for Functional Axon Regeneration of Adult DRG Neurons upon SNL In Vivo

(A and B) Analysis of regeneration of sensory axons by SCG10 immunostaining at SNL D3. Shown are sample images of regenerating sensory axons identified by SCG10 (A) (scale bar, 500 μm) and quantification (B). SCG10 immunofluorescence intensity was measured at different distal distances and normalized to that at the lesion site as the regenerative index. Values represent mean ± SEM (n = 5 for each group; *p < 0.05; two-way ANOVA).

(C–E) Analysis of regenerating axons visualized by GFP labeling at SNL D7. Cross-sections of sciatic nerves at −1 to 6 mm distal to the lesion site from AAV-Ctrl and AAV-Tet3 KD treated animals were analyzed. Shown are sample images of GFP and Tuj1 (C) (scale bar, 300 μm) and quantification (D and E). Values represent mean ± SEM (n = 3–4 for each group; *p < 0.05; two-way ANOVA).

(F and G) Assay of re-innervation of epidermal area of the hindpaw by regenerating sensory axons. Shown in (F) are the schematic diagram and sample images of cross sections of hindpaw glabrous skin of Ctrl and Tet3 KD mice immunostained with the pan neuronal marker PGP9.5. The dotted line indicates the border between dermis and epidermis. Scale bar, 20 μm. Also shown are quantifications of the number of intraepidermal nerve fibers in a 1 mm segment of different epidermal areas (G). Values represent mean ± SEM (n = 4 for each group; **p < 0.01; *p < 0.05; n.s. p > 0.1; two-way ANOVA).

(H) Assessment of thermal sensory recovery after SNL in AAV-Ctrl and AAV-Tet3 KD treated animals. Values represent mean ± SEM (n = 9–12 animals per group; **p < 0.01; ***p < 0.001; two-way ANOVA).

sucrose cushion method (Kozlenkov et al., 2014). We initially used methylation-sensitive restriction enzyme cutting coupled with qPCR to screen CC^{m}GG sites and quantify their methylation levels (Guo et al., 2011a). While the *ATF3* promoter was not methylated, multiple CC^{m}GG sites in the gene body and distal enhancer regions (DE1–DE4) were hypermethylated and exhibited a significant decrease in methylation levels upon SNL at D1 (Figure S3C). One recent study showed that injuries upregulate c-Myc expression in DRGs but not in retinal ganglion cells (RGCs), and forced c-Myc expression promotes axon regeneration of RGCs after optic nerve injury (Belin et al., 2015). Interestingly, significant DNA demethylation was also observed at putative *c-Myc* distal enhancer sites (Figure S3D). To ensure that DNA demethylation indeed occurred in neurons, we performed bisulfite-sequencing from NeuN^{+} nuclei purified by fluorescence-activated cell sorting (FACS). We found a significant decrease in methylation levels at multiple CpG sites within DE1–DE2 regions of *ATF3* at SNL D1 (Figure S3E). In contrast, we did not observe any demethylation within the *GAP43* loci from the same neuronal samples (Figure S3F). Therefore, injury-induced DNA demethylation in adult DRG neurons appears to be region-specific.

To determine the specific role of Tet3 in injury-induced DNA demethylation, we engineered AAV to co-express H2B-GFP and shRNA in adult DRGs in vivo and FACS-purified eight groups of NeuN^{+} nuclei: GFP^{-} uninfected neurons or GFP^{+} neurons expressing either Ctrl-shRNA or Tet3-shRNA, under either naive or SNL D1 conditions (Figure 3E). Due to the limited material for bisulfite-sequencing analysis, we focused on the *ATF3* DE1 region. Quantitative analysis from three independent experiments showed that SNL induced significant DNA demethylation in both GFP^{+} and GFP^{-} neurons following injection of AAV expressing Ctrl-shRNA and GFP (Figures 3E and 3F). In contrast, upon injection of AAV expressing Tet3-shRNA and GFP, GFP^{+} neurons showed minimal changes in methylation levels, whereas GFP^{-} neurons still exhibited SNL-induced demethylation at these CpG sites from the

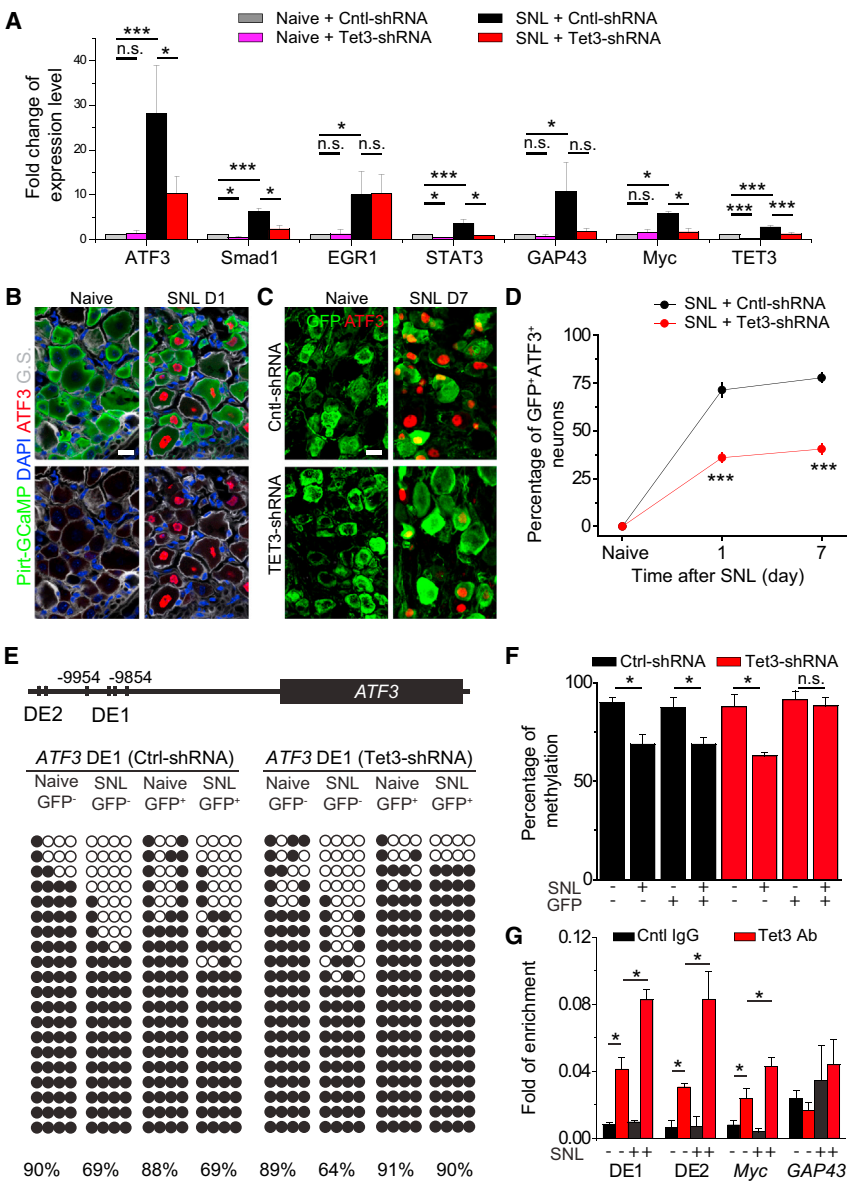

Figure 3. Tet3 Regulates the Expression of Multiple Injury-Induced RAGs and Mediates Active DNA Demethylation of *ATF3* Genomic Regions

(A) Analysis of expression of some known RAGs. The mRNA expression was assessed by qPCR at SNL D1 and compared to the Ctrl naive group. Values represent mean ± SEM (n = 3 for each group; ***p < 0.001; *p < 0.05; n.s. p > 0.1; two-way ANOVA).

(B–D) Assessment of ATF3 induction in Tet3 KD DRGs at SNL D1 and D7. Shown are sample images of immunostaining for GFP, ATF3, and glutamine synthetase (G.S.) in Pirt-GCAMP3 neuronal reporter mice (B) and for ATF3 and GFP in normal mice (C) and quantifications (D). Scale bars, 20 μm. Values represent mean ± SEM (n = 4 for each group; ***p < 0.001; two-way ANOVA).

(E and F) Methylation status of the *ATF3* distal enhancer region 1 (DE1) in Ctrl and Tet3 KD DRG neurons. AAV transduced (GFP^+) and non-transduced (GFP^-) $NeuN^+$ neurons from L4 and L5 DRGs at SNL D1 were isolated by FACS and subjected to bisulfite sequencing analysis. (E) Sample reads of individual alleles. Open circles indicate unmethylated cytosines and closed circles indicate methylated cytosines. (F) Summary from three independent biological replicates with at least 20 alleles each. Values represent mean ± SEM (n = 3 for each group; *p < 0.05; two-way ANOVA).

(G) ChIP-qPCR analysis of Tet3 binding to different genomic regions that were also examined for DNA methylation levels (as shown in Figure S3C). Values represent mean ± SEM (n = 3 for each group; *p < 0.05; two-way ANOVA).

same DRGs (Figures 3E and 3F). Furthermore, chromatin immunoprecipitation (ChIP) analysis using anti-Tet3 antibodies (Jin et al., 2016) showed enriched Tet3 binding at the DE1 and DE2 regions of the *ATF3* gene, which was further enhanced upon SNL (Figure 3G). We also observed similar binding properties of Tet3 to the *c-Myc* locus but not to the *GAP43* locus (Figure 3G). Together, these results suggest a model wherein peripheral nerve injury leads to enhanced recruitment of Tet3 to methylated CpG sites of enhancers of RAGs followed by demethylation of these CpG sites, resulting in upregulated gene expression.

TDG Coordinates with Tet3 to Regulate RAG Expression and Axon Regeneration

Tet family proteins have been shown to exert functions independent of DNA demethylation activity (Chen et al., 2013; Williams et al., 2011). In addition, 5hmC has been proposed as a signaling mechanism itself via its binding partners (Iurlaro et al., 2013; Mellén et al., 2012; Spruijt et al., 2013). Transient elevation of 5hmC upon injury is consistent with its role as an intermediate of active DNA demethylation (Figure 1D). We further examined the role of TDG, a critical downstream mediator of active DNA demethylation (Bellacosa and Drohat, 2015; Wu and Zhang, 2014; Cortellino et al., 2011) (Figure S4A), in SNL-induced intrinsic axon regeneration competence. Upon TDG KD (Figure S4B), axonal regeneration was significantly reduced at SNL D7 (Figures 4A and 4B). We confirmed our results via AAV-mediated co-expression of GFP and Cre in DRGs of adult $Tdg^{f/f}$ mice (Figures 4C and 4D).

To investigate further whether Tet3 and TDG share the same molecular mechanisms in regulating axon regeneration, we evaluated the expression of known RAGs in TDG KD samples. SNL-induced ATF3 expression was attenuated in TDG KD neurons at both SNL D1 and D7, similar to the effect of Tet3 KD (Figures 4E and 4F). qPCR analysis of DRGs at SNL D1 showed that TDG KD attenuated the induction of a similar subset of RAGs as Tet3 KD (Figure 4G). Tet proteins generate 5hmC, 5fC, and 5caC through iterative oxidation of 5mC, whereas TDG excises 5fC and 5caC to initiate base-excision repair to complete the DNA

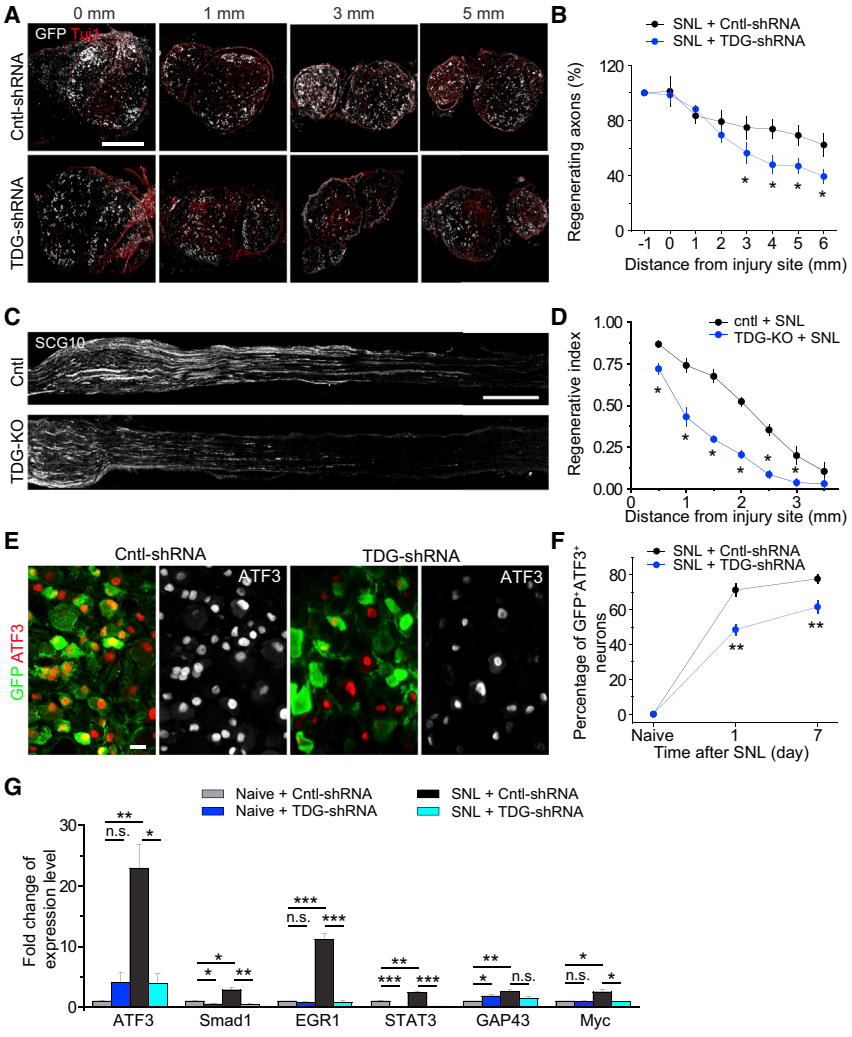

Figure 4. TDG Is Required for SNL-Induced Axon Regeneration and ATF3 Expression in Adult DRG Neurons

(A–D) In vivo axon regeneration assay. Similar to Figures 2C and 2D, shown are sample images (A) (scale bar, 300 μm) and quantification (B) at SNL D7 with expression of control-shRNA or TDG-shRNA. The same data from Ctrl-shRNA in Figure 2C is replotted for comparison. Similar to Figures 2A and 2B, also shown are sample images of regenerating sensory axons identified by SCG10 (C) (scale bar, 500 μm) in *TDG*$^{f/f}$ mice expressing GFP (Ctrl), or GFP and Cre (TDG-KO) and quantifications (D). Values represent mean ± SEM (n = 4 for each group; *p < 0.05; two-way ANOVA).

(E and F) Assessment of ATF3 induction in TDG KD DRGs. Similar to Figure 3B, shown are sample images (E) (scale bar, 20 μm) and quantifications (F). Values represent mean ± SEM (n = 4 for each group; **p < 0.01; two-way ANOVA).

(G) TDG-dependent expression of multiple SNL-induced RAGs. The mRNA expression was assessed by qPCR at SNL D1 and compared to the Ctrl naive group. Values represent mean ± SEM (n = 3 for each group; ***p < 0.001; **p < 0.01; *p < 0.05; n.s. p > 0.1; two-way ANOVA).

demethylation process (Figure S4A). While Tet3 KD blocked SNL-induced 5hmC level increases (Figure 1F), TDG KD led to a further increase of 5hmC levels at SNL D7 (Figures S4C and S4D). These results suggest that the complete DNA demethylation process, not SNL-induced 5hmC increase alone, primarily mediates the induction of RAGs and unlocks the axonal growth capacity of mature DRG neurons.

Tet1 Is Involved in PTEN Deletion-Induced Retinal Ganglion Neuron Axon Regeneration

To assess whether active DNA demethylation is also required for axon regeneration in the adult CNS, we employed the model of PTEN deletion-induced axon regeneration of RGCs in adult mice (Park et al., 2008). We co-expressed Cre and shRNA for Tet1, Tet2, or Tet3, in adult RGCs, followed by axotomy and axonal labeling (Park et al., 2008). Interestingly, expression of shRNA-Tet1, but not shRNA-Tet2 or shRNA-Tet3, attenuated axonal regeneration of RGCs in comparison to the shRNA-control (Figure 5). Therefore, Tet signaling is also required for induced axon regeneration in the adult CNS with the specific involvement of Tet1.

DISCUSSION

In addition to the extrinsic barrier imposed by the inhibitory environment (He and Koprivica, 2004; Silver et al., 2014), poor intrinsic growth capacity of mature CNS neurons is a major contributing factor to regeneration failure (Liu et al., 2011). Therefore, defining how injured mature PNS neurons switch to a pro-regenerative state may not only reveal the basic biology of mature mammalian neurons, but may also suggest novel therapeutic strategies for promoting axon regeneration within both the PNS and CNS. Our results support a model wherein peripheral nerve injury, via retrograde Ca^{2+} signaling, upregulates Tet3 expression and the active DNA demethylation pathway, which in turn removes an intrinsic barrier to the expression of an ensemble of RAGs and to functional axon regeneration of mature PNS neurons in vivo (Figure S5). Our initial study also suggests a similar intrinsic epigenetic barrier of DNA methylation for induced axon regeneration in the adult CNS.

Large-scale and long-lasting changes in the expression of RAGs after injury have been associated with the regenerative capacity of mature PNS neurons. Epigenetic mechanisms, such as DNA demethylation, are well-suited to orchestrate transcriptional re-activation of a large repertoire of RAGs over an extended period of time. Many RAGs, including ATF3 and c-Myc, exhibit developmentally regulated expression patterns and diminished expression in mature neurons (Figure 3A), which might be maintained via DNA methylation. Indeed, we found that at putative enhancer regions of both *ATF3* and *c-Myc*, multiple loci are hypermethylated in mature DRG neurons under basal

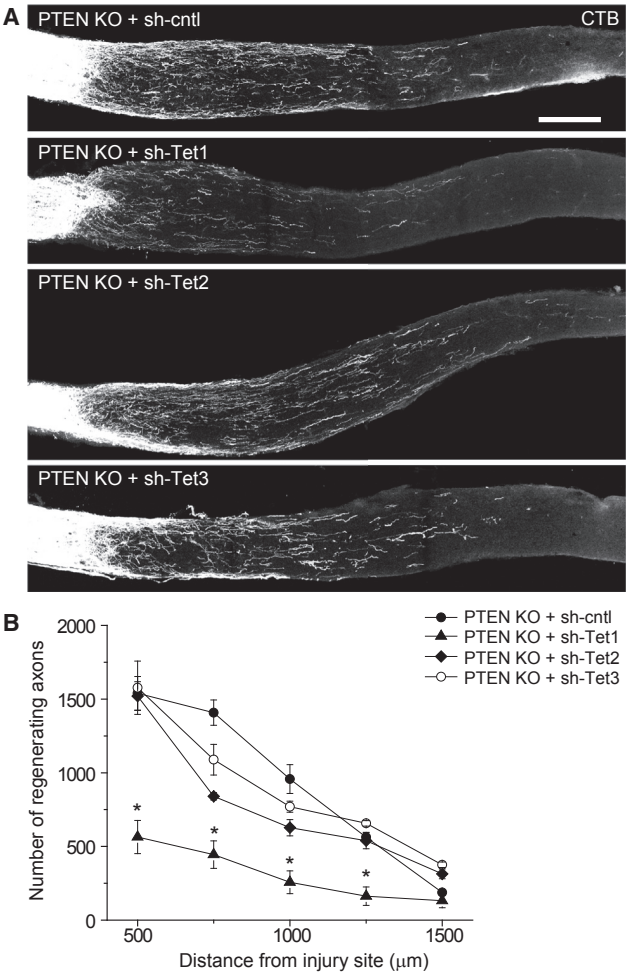

Figure 5. Tet1 Is Required for Pten Deletion-Induced Axon Regeneration of Retinal Ganglion Neurons in the Adult Mouse

Adult *Pten*$^{f/f}$ mice were injected with AAVs to co-express GFP, Cre, and control shRNA, or shRNA against Tet1, Tet2, or Tet3 in the eye, followed by optic nerve crush 2 weeks later. RGC axons were anterogradely labeled by cholera toxin β subunit 12 days after injury. Shown are sample images of labeled axons (A) (scale bar, 20 μm) and quantifications (B). Values represent mean ± SEM (n = 3 for each group; *p < 0.05; two-way ANOVA).

conditions and associated with very low expression levels. Upon SNL injury, there is an enhanced binding of Tet3 to these regions, accompanied by demethylation and induced gene expression. How Tet3 is targeted to these specific regions and how its binding is enhanced upon injury remain to be determined. One recent study published during the revision of this paper profiled 5hmC from the whole adult mouse DRGs and found large-scale changes, including regions associated with RAGs (Loh et al., 2017). Interestingly, peripheral injury triggers differential 5hmC changes that are associated with distinct signaling pathways compared to injury of the central branch of DRG neurons, which does not result in axon regeneration. Because of tremendous cellular heterogeneity in the adult mouse nervous system, genome-wide methylation and hydroxymethylation analysis of a particular neuronal type of limited quantity in vivo remains a technical challenge (Shin et al., 2014a). Here, we purified DRG neurons from adult mice and focused on a few candidate genes as a proof of principle. Future technological developments may enable analysis of DNA methylomes in very small populations of defined cell types and contribute to a more comprehensive understanding of 5hmC/5mC dynamics in the regulation of RAG expression in neurons.

Tet function and DNA demethylation have been shown to promote other cellular reprogramming processes, such as reprogramming of somatic cells into pluripotency, although expression of Tet proteins alone is not sufficient (Bagci and Fisher, 2013). Here, we show that DNA demethylation removes one of the major barriers for axon regeneration, but it is likely not sufficient to switch mature neurons from a dormant state to an active axonal growth state. Instead, DNA demethylation may coordinate with other epigenetic mechanisms (Trakhtenberg and Goldberg, 2012), such as histone acetylation, which has been shown to promote PNS axon regeneration (Cho et al., 2013; Finelli et al., 2013; Gaub et al., 2011; Puttagunta et al., 2014). Interestingly, enhancing histone acetylation using HDAC inhibitors is not sufficient to turn on the expression of ATF3 and Smad1 in adult DRGs (Finelli et al., 2013), two genes that we found to be regulated by Tet3 and TDG (Figures 3A and 4G). Future studies will address how different epigenetic mechanisms coordinate to reactivate the robust axonal growth state. Notably, Tet proteins are known to interact with multiple chromatin regulators to modulate gene expression (Chen et al., 2013; Deplus et al., 2013; Perera et al., 2015).

In summary, our study identifies DNA methylation as an intrinsic barrier for functional regeneration of mature mammalian neurons. Different from recent studies of cell identity reprogramming (Arlotta and Berninger, 2014), our finding of a critical role of an epigenetic DNA modification mechanism in reprogramming mature neurons to an axon regeneration-competent state, without altering cell identity, extends the classic concept of reprogramming and may have broad implications for regenerative medicine.

STAR★METHODS

Detailed methods are provided in the online version of this paper and include the following:

- KEY RESOURCES TABLE
- CONTACT FOR REAGENT AND RESOURCE SHARING
- EXPERIMENTAL MODEL AND SUBJECT DETAILS
  - Animals
- METHOD DETAILS
  - AAV constructs
  - DRG cultures and neurite outgrowth assay
  - Animal surgery
  - Behavioral analysis
  - In situ hybridization
  - Western blot analysis
  - Gene expression and methylation analyses
  - In vivo DRG axon regeneration assay
  - Immunohistology

SUPPLEMENTAL INFORMATION

Supplemental Information includes five figures and one table and can be found with this article online at http://dx.doi.org/10.1016/j.neuron.2017.03.034.

AUTHOR CONTRIBUTIONS

Y.-L.W. led the project and was involved in all aspects of the study. R.A. performed surgical procedures and data quantification for DRG studies. J.C. led bisulfite sequencing and molecular analyses. J.J. performed western blot analysis and along with C.Z. contributed to other data collection. C.W. and Z.H. performed RGC experiments. R.M. and A.H. contributed to behavioral experimental design and testing. S.-G.J. and G.P.P. provided Tet3 antibodies for ChIP analysis. A.B. contributed $Tdg^{f/f}$ mice. X.D. contributed Pirt-GCaMP3 reporter mice. Y.L.W., H.S., and G.M. designed the project, analyzed the data, and wrote the paper. All authors helped prepare the manuscript.

ACKNOWLEDGMENTS

We thank Dr. Hongyan Zou, members of Ming and Song laboratories, and The Dr. Miriam and Sheldon G. Adelson Medical Research Foundation (AMRF) investigators for discussion, and Y. Cai and L. Liu for technical support. This work was supported by grants from AMRF (to G.M., Z.H., and A.H.) and from NIH (P01NS097206 to H.S., R35NS097370 to G.M., R01CA160965 to G.P.P., R01CA78412 to A.B., and P30CA06927 to Fox Chase Cancer Center).

Received: September 24, 2016
Revised: February 5, 2017
Accepted: March 23, 2017
Published: April 19, 2017

REFERENCES

Arlotta, P., and Berninger, B. (2014). Brains in metamorphosis: reprogramming cell identity within the central nervous system. Curr. Opin. Neurobiol. *27*, 208–214.

Bagci, H., and Fisher, A.G. (2013). DNA demethylation in pluripotency and reprogramming: the role of tet proteins and cell division. Cell Stem Cell *13*, 265–269.

Befort, K., Karchewski, L., Lanoue, C., and Woolf, C.J. (2003). Selective up-regulation of the growth arrest DNA damage-inducible gene Gadd45 alpha in sensory and motor neurons after peripheral nerve injury. Eur. J. Neurosci. *18*, 911–922.

Belin, S., Nawabi, H., Wang, C., Tang, S., Latremoliere, A., Warren, P., Schorle, H., Uncu, C., Woolf, C.J., He, Z., and Steen, J.A. (2015). Injury-induced decline of intrinsic regenerative ability revealed by quantitative proteomics. Neuron *86*, 1000–1014.

Bellacosa, A., and Drohat, A.C. (2015). Role of base excision repair in maintaining the genetic and epigenetic integrity of CpG sites. DNA Repair (Amst.) *32*, 33–42.

Bonaguidi, M.A., Wheeler, M.A., Shapiro, J.S., Stadel, R.P., Sun, G.J., Ming, G.L., and Song, H. (2011). In vivo clonal analysis reveals self-renewing and multipotent adult neural stem cell characteristics. Cell *145*, 1142–1155.

Chen, Q., Chen, Y., Bian, C., Fujiki, R., and Yu, X. (2013). TET2 promotes histone O-GlcNAcylation during gene transcription. Nature *493*, 561–564.

Cho, Y., and Cavalli, V. (2014). HDAC signaling in neuronal development and axon regeneration. Curr. Opin. Neurobiol. *27*, 118–126.

Cho, Y., Sloutsky, R., Naegle, K.M., and Cavalli, V. (2013). Injury-induced HDAC5 nuclear export is essential for axon regeneration. Cell *155*, 894–908.

Cortellino, S., Xu, J., Sannai, M., Moore, R., Caretti, E., Cigliano, A., Le Coz, M., Devarajan, K., Wessels, A., Soprano, D., et al. (2011). Thymine DNA glycosylase is essential for active DNA demethylation by linked deamination-base excision repair. Cell *146*, 67–79.

Costigan, M., Befort, K., Karchewski, L., Griffin, R.S., D'Urso, D., Allchorne, A., Sitarski, J., Mannion, J.W., Pratt, R.E., and Woolf, C.J. (2002). Replicate high-density rat genome oligonucleotide microarrays reveal hundreds of regulated genes in the dorsal root ganglion after peripheral nerve injury. BMC Neurosci. *3*, 16.

Delree, P., Leprince, P., Schoenen, J., and Moonen, G. (1989). Purification and culture of adult rat dorsal root ganglia neurons. J. Neurosci. Res. *23*, 198–206.

Deplus, R., Delatte, B., Schwinn, M.K., Defrance, M., Méndez, J., Murphy, N., Dawson, M.A., Volkmar, M., Putmans, P., Calonne, E., et al. (2013). TET2 and TET3 regulate GlcNAcylation and H3K4 methylation through OGT and SET1/COMPASS. EMBO J. *32*, 645–655.

Di Maio, A., Skuba, A., Himes, B.T., Bhagat, S.L., Hyun, J.K., Tessler, A., Bishop, D., and Son, Y.J. (2011). In vivo imaging of dorsal root regeneration: rapid immobilization and presynaptic differentiation at the CNS/PNS border. J. Neurosci. *31*, 4569–4582.

Duan, X., Chang, J.H., Ge, S., Faulkner, R.L., Kim, J.Y., Kitabatake, Y., Liu, X.B., Yang, C.H., Jordan, J.D., Ma, D.K., et al. (2007). Disrupted-In-Schizophrenia 1 regulates integration of newly generated neurons in the adult brain. Cell *130*, 1146–1158.

Fagoe, N.D., Attwell, C.L., Kouwenhoven, D., Verhaagen, J., and Mason, M.R. (2015). Overexpression of ATF3 or the combination of ATF3, c-Jun, STAT3 and Smad1 promotes regeneration of the central axon branch of sensory neurons but without synergistic effects. Hum. Mol. Genet. *24*, 6788–6800.

Feng, J., Shao, N., Szulwach, K.E., Vialou, V., Huynh, J., Zhong, C., Le, T., Ferguson, D., Cahill, M.E., Li, Y., et al. (2015). Role of Tet1 and 5-hydroxymethylcytosine in cocaine action. Nat. Neurosci. *18*, 536–544.

Finelli, M.J., Wong, J.K., and Zou, H. (2013). Epigenetic regulation of sensory axon regeneration after spinal cord injury. J. Neurosci. *33*, 19664–19676.

Gaub, P., Joshi, Y., Wuttke, A., Naumann, U., Schnichels, S., Heiduschka, P., and Di Giovanni, S. (2011). The histone acetyltransferase p300 promotes intrinsic axonal regeneration. Brain *134*, 2134–2148.

Goldberg, J.L., Klassen, M.P., Hua, Y., and Barres, B.A. (2002). Amacrine-signaled loss of intrinsic axon growth ability by retinal ganglion cells. Science *296*, 1860–1864.

Gräff, J., Kim, D., Dobbin, M.M., and Tsai, L.H. (2011). Epigenetic regulation of gene expression in physiological and pathological brain processes. Physiol. Rev. *91*, 603–649.

Guo, J.U., Ma, D.K., Mo, H., Ball, M.P., Jang, M.H., Bonaguidi, M.A., Balazer, J.A., Eaves, H.L., Xie, B., Ford, E., et al. (2011a). Neuronal activity modifies the DNA methylation landscape in the adult brain. Nat. Neurosci. *14*, 1345–1351.

Guo, J.U., Su, Y., Zhong, C., Ming, G.L., and Song, H. (2011b). Emerging roles of TET proteins and 5-hydroxymethylcytosines in active DNA demethylation and beyond. Cell Cycle *10*, 2662–2668.

Guo, J.U., Su, Y., Zhong, C., Ming, G.L., and Song, H. (2011c). Hydroxylation of 5-methylcytosine by TET1 promotes active DNA demethylation in the adult brain. Cell *145*, 423–434.

Guo, J.U., Szulwach, K.E., Su, Y., Li, Y., Yao, B., Xu, Z., Shin, J.H., Xie, B., Gao, Y., Ming, G.L., et al. (2014). Genome-wide antagonism between 5-hydroxymethylcytosine and DNA methylation in the adult mouse brain. Front. Biol. (Beijing) *9*, 66–74.

Hammarlund, M., and Jin, Y. (2014). Axon regeneration in C. elegans. Curr. Opin. Neurobiol. *27*, 199–207.

He, Z., and Jin, Y. (2016). Intrinsic control of axon regeneration. Neuron *90*, 437–451.

He, Z., and Koprivica, V. (2004). The Nogo signaling pathway for regeneration block. Annu. Rev. Neurosci. *27*, 341–368.

He, Y.F., Li, B.Z., Li, Z., Liu, P., Wang, Y., Tang, Q., Ding, J., Jia, Y., Chen, Z., Li, L., et al. (2011). Tet-mediated formation of 5-carboxylcytosine and its excision by TDG in mammalian DNA. Science *333*, 1303–1307.

Iskandar, B.J., Rizk, E., Meier, B., Hariharan, N., Bottiglieri, T., Finnell, R.H., Jarrard, D.F., Banerjee, R.V., Skene, J.H., Nelson, A., et al. (2010). Folate regulation of axonal regeneration in the rodent central nervous system through DNA methylation. J. Clin. Invest. *120*, 1603–1616.

Ito, S., Shen, L., Dai, Q., Wu, S.C., Collins, L.B., Swenberg, J.A., He, C., and Zhang, Y. (2011). Tet proteins can convert 5-methylcytosine to 5-formylcytosine and 5-carboxylcytosine. Science *333*, 1300–1303.

Iurlaro, M., Ficz, G., Oxley, D., Raiber, E.A., Bachman, M., Booth, M.J., Andrews, S., Balasubramanian, S., and Reik, W. (2013). A screen for hydroxymethylcytosine and formylcytosine binding proteins suggests functions in transcription and chromatin regulation. Genome Biol. *14*, R119.

Jaenisch, R., and Bird, A. (2003). Epigenetic regulation of gene expression: how the genome integrates intrinsic and environmental signals. Nat. Genet. *33* (*Suppl*), 245–254.

Jang, M.H., Bonaguidi, M.A., Kitabatake, Y., Sun, J., Song, J., Kang, E., Jun, H., Zhong, C., Su, Y., Guo, J.U., et al. (2013). Secreted frizzled-related protein 3 regulates activity-dependent adult hippocampal neurogenesis. Cell Stem Cell *12*, 215–223.

Jin, S.G., Zhang, Z.M., Dunwell, T.L., Harter, M.R., Wu, X., Johnson, J., Li, Z., Liu, J., Szabó, P.E., Lu, Q., et al. (2016). Tet3 reads 5-carboxylcytosine through its CXXC domain and is a potential guardian against neurodegeneration. Cell Rep. *14*, 493–505.

Kaas, G.A., Zhong, C., Eason, D.E., Ross, D.L., Vachhani, R.V., Ming, G.L., King, J.R., Song, H., and Sweatt, J.D. (2013). TET1 controls CNS 5-methylcytosine hydroxylation, active DNA demethylation, gene transcription, and memory formation. Neuron *79*, 1086–1093.

Kim, Y.S., Anderson, M., Park, K., Zheng, Q., Agarwal, A., Gong, C., Saijilafu, Young, L., He, S., LaVinka, P.C., et al. (2016). Coupled activation of primary sensory neurons contributes to chronic pain. Neuron *91*, 1085–1096.

Kozlenkov, A., Roussos, P., Timashpolsky, A., Barbu, M., Rudchenko, S., Bibikova, M., Klotzle, B., Byne, W., Lyddon, R., Di Narzo, A.F., et al. (2014). Differences in DNA methylation between human neuronal and glial cells are concentrated in enhancers and non-CpG sites. Nucleic Acids Res. *42*, 109–127.

Lister, R., Mukamel, E.A., Nery, J.R., Urich, M., Puddifoot, C.A., Johnson, N.D., Lucero, J., Huang, Y., Dwork, A.J., Schultz, M.D., et al. (2013). Global epigenomic reconfiguration during mammalian brain development. Science *341*, 1237905.

Liu, K., Lu, Y., Lee, J.K., Samara, R., Willenberg, R., Sears-Kraxberger, I., Tedeschi, A., Park, K.K., Jin, D., Cai, B., et al. (2010). PTEN deletion enhances the regenerative ability of adult corticospinal neurons. Nat. Neurosci. *13*, 1075–1081.

Liu, K., Tedeschi, A., Park, K.K., and He, Z. (2011). Neuronal intrinsic mechanisms of axon regeneration. Annu. Rev. Neurosci. *34*, 131–152.

Loh, Y.E., Koemeter-Cox, A., Finelli, M.J., Shen, L., Friedel, R.H., and Zou, H. (2017). Comprehensive mapping of 5-hydroxymethylcytosine epigenetic dynamics in axon regeneration. Epigenetics *12*, 77–92.

Ma, D.K., Jang, M.H., Guo, J.U., Kitabatake, Y., Chang, M.L., Pow-Anpongkul, N., Flavell, R.A., Lu, B., Ming, G.L., and Song, H. (2009). Neuronal activity-induced Gadd45b promotes epigenetic DNA demethylation and adult neurogenesis. Science *323*, 1074–1077.

Ma, D.K., Marchetto, M.C., Guo, J.U., Ming, G.L., Gage, F.H., and Song, H. (2010). Epigenetic choreographers of neurogenesis in the adult mammalian brain. Nat. Neurosci. *13*, 1338–1344.

Mellén, M., Ayata, P., Dewell, S., Kriaucionis, S., and Heintz, N. (2012). MeCP2 binds to 5hmC enriched within active genes and accessible chromatin in the nervous system. Cell *151*, 1417–1430.

Moore, D.L., and Goldberg, J.L. (2011). Multiple transcription factor families regulate axon growth and regeneration. Dev. Neurobiol. *71*, 1186–1211.

Park, K.K., Liu, K., Hu, Y., Smith, P.D., Wang, C., Cai, B., Xu, B., Connolly, L., Kramvis, I., Sahin, M., and He, Z. (2008). Promoting axon regeneration in the adult CNS by modulation of the PTEN/mTOR pathway. Science *322*, 963–966.

Perera, A., Eisen, D., Wagner, M., Laube, S.K., Künzel, A.F., Koch, S., Steinbacher, J., Schulze, E., Splith, V., Mittermeier, N., et al. (2015). TET3 is recruited by REST for context-specific hydroxymethylation and induction of gene expression. Cell Rep. *11*, 283–294.

Puttagunta, R., Tedeschi, A., Sória, M.G., Hervera, A., Lindner, R., Rathore, K.I., Gaub, P., Joshi, Y., Nguyen, T., Schmandke, A., et al. (2014). PCAF-dependent epigenetic changes promote axonal regeneration in the central nervous system. Nat. Commun. *5*, 3527.

Rishal, I., and Fainzilber, M. (2014). Axon-soma communication in neuronal injury. Nat. Rev. Neurosci. *15*, 32–42.

Rossi, F., Gianola, S., and Corvetti, L. (2007). Regulation of intrinsic neuronal properties for axon growth and regeneration. Prog. Neurobiol. *81*, 1–28.

Rudenko, A., Dawlaty, M.M., Seo, J., Cheng, A.W., Meng, J., Le, T., Faull, K.F., Jaenisch, R., and Tsai, L.H. (2013). Tet1 is critical for neuronal activity-regulated gene expression and memory extinction. Neuron *79*, 1109–1122.

Seijffers, R., Mills, C.D., and Woolf, C.J. (2007). ATF3 increases the intrinsic growth state of DRG neurons to enhance peripheral nerve regeneration. J. Neurosci. *27*, 7911–7920.

Shin, J.E., Cho, Y., Beirowski, B., Milbrandt, J., Cavalli, V., and DiAntonio, A. (2012). Dual leucine zipper kinase is required for retrograde injury signaling and axonal regeneration. Neuron *74*, 1015–1022.

Shin, J., Ming, G.L., and Song, H. (2014a). Decoding neural transcriptomes and epigenomes via high-throughput sequencing. Nat. Neurosci. *17*, 1463–1475.

Shin, J., Ming, G.L., and Song, H. (2014b). DNA modifications in the mammalian brain. Philos. Trans. R. Soc. Lond. B Biol. Sci. *369*, http://dx.doi.org/10.1098/rstb.2013.0512.

Shin, J.E., Geisler, S., and DiAntonio, A. (2014c). Dynamic regulation of SCG10 in regenerating axons after injury. Exp. Neurol. *252*, 1–11.

Silver, J., Schwab, M.E., and Popovich, P.G. (2014). Central nervous system regenerative failure: role of oligodendrocytes, astrocytes, and microglia. Cold Spring Harb. Perspect. Biol. *7*, a020602.

Smith, D.S., and Skene, J.H. (1997). A transcription-dependent switch controls competence of adult neurons for distinct modes of axon growth. J. Neurosci. *17*, 646–658.

Song, J., Zhong, C., Bonaguidi, M.A., Sun, G.J., Hsu, D., Gu, Y., Meletis, K., Huang, Z.J., Ge, S., Enikolopov, G., et al. (2012). Neuronal circuitry mechanism regulating adult quiescent neural stem-cell fate decision. Nature *489*, 150–154.

Spruijt, C.G., Gnerlich, F., Smits, A.H., Pfaffeneder, T., Jansen, P.W., Bauer, C., Münzel, M., Wagner, M., Müller, M., Khan, F., et al. (2013). Dynamic readers for 5-(hydroxy)methylcytosine and its oxidized derivatives. Cell *152*, 1146–1159.

Tahiliani, M., Koh, K.P., Shen, Y., Pastor, W.A., Bandukwala, H., Brudno, Y., Agarwal, S., Iyer, L.M., Liu, D.R., Aravind, L., and Rao, A. (2009). Conversion of 5-methylcytosine to 5-hydroxymethylcytosine in mammalian DNA by MLL partner TET1. Science *324*, 930–935.

Tedeschi, A., and Bradke, F. (2017). Spatial and temporal arrangement of neuronal intrinsic and extrinsic mechanisms controlling axon regeneration. Curr. Opin. Neurobiol. *42*, 118–127.

Thakur, M., Crow, M., Richards, N., Davey, G.I., Levine, E., Kelleher, J.H., Agley, C.C., Denk, F., Harridge, S.D., and McMahon, S.B. (2014). Defining the nociceptor transcriptome. Front. Mol. Neurosci. *7*, 87.

Trakhtenberg, E.F., and Goldberg, J.L. (2012). Epigenetic regulation of axon and dendrite growth. Front. Mol. Neurosci. *5*, 24.

Weng, Y.L., Joseph, J., An, R., Song, H., and Ming, G.L. (2016). Epigenetic regulation of axonal regenerative capacity. Epigenomics *8*, 1429–1442.

Williams, K., Christensen, J., Pedersen, M.T., Johansen, J.V., Cloos, P.A., Rappsilber, J., and Helin, K. (2011). TET1 and hydroxymethylcytosine in transcription and DNA methylation fidelity. Nature *473*, 343–348.

Wong, J.K., and Zou, H. (2014). Reshaping the chromatin landscape after spinal cord injury. Front. Biol. (Beijing) *9*, 356–366.

Wright, M.C., Mi, R., Connor, E., Reed, N., Vyas, A., Alspalter, M., Coppola, G., Geschwind, D.H., Brushart, T.M., and Höke, A. (2014). Novel roles for osteopontin and clusterin in peripheral motor and sensory axon regeneration. J. Neurosci. *34*, 1689–1700.

Wu, H., and Zhang, Y. (2014). Reversing DNA methylation: mechanisms, genomics, and biological functions. Cell *156*, 45–68.

Yao, B., Christian, K.M., He, C., Jin, P., Ming, G.L., and Song, H. (2016). Epigenetic mechanisms in neurogenesis. Nat. Rev. Neurosci. *17*, 537–549.

Yu, H., Su, Y., Shin, J., Zhong, C., Guo, J.U., Weng, Y.L., Gao, F., Geschwind, D.H., Coppola, G., Ming, G.L., and Song, H. (2015). Tet3 regulates synaptic transmission and homeostatic plasticity via DNA oxidation and repair. Nat. Neurosci. *18*, 836–843.

Zhou, F.Q., and Snider, W.D. (2006). Intracellular control of developmental and regenerative axon growth. Philos. Trans. R. Soc. Lond. B Biol. Sci. *361*, 1575–1592.

STAR★METHODS

KEY RESOURCES TABLE

REAGENT or RESOURCE	SOURCE	IDENTIFIER
Antibodies		
Mouse anti- β-tubulin (Tuj1)	BioLegend	801202; RRID: AB_10063408
Mouse anti- β-tubulin (Tuj1)	Sigma	T8328
Alkaline phosphatase-conjugated anti-digoxygenin antibody	Roche	11093274910; RRID: AB_514497
Mouse anti-phospho-c-Jun	Cell Signaling	9261S; RRID: AB_2130162
Rabbit anti-5hmC	Active Motif	39769; RRID: AB_10013602
Rabbit anti-ATF3	Santa Cruz	sc-188; RRID: AB_2258513
Rabbit anti-PGP9.5	AbD Serotec	7863-0504; RRID: AB_2210505
Goat anti-GFP	Rockland	600-101215; RRID: AB_218182
Mouse anti-Glutamine Synthetase	Santa Cruz	sc-74430; RRID: AB_1127501
Mouse Anti-NeuN	Millipore	MAB377B; RRID: AB_177621
Rabbit anti-SCG10	Novus Biologicals	NBP1-49461; RRID: AB_10011569
Mouse anti-Tet3	Abiocode	M1092-4a
Cy2–conjugated secondary	Jackson ImmunoResearch	705-225-147
Cy3–conjugated secondary	Jackson ImmunoResearch	711-165-152
Cy5–conjugated secondary	Jackson ImmunoResearch	715-175-150
Rabbit anti-cleaved caspase 3	Invitrogen	9H19L2; RRID: AB_2532293
HRP-conjugated goat anti-mouse IgG	Santa Cruz	sc-2031; RRID: AB_631737
HRP-conjugated goat anti-rabbit IgG	Santa Cruz	sc-2004; RRID: AB_631746
Rabbit anti-GAPDH	Abcam	Ab9485; RRID: AB_307275
Rabbit IgG	Cell Signaling	2729; RRID: AB_1031062
Chemicals, Peptides, and Recombinant Proteins		
Collagenase II	Worthington Biochemical Corporation	LS004112
Dispase	Worthington Biochemical Corporation	LS02100
TRIzol	Invitrogen	15596018
Fast SYBR Green Master Mix	ABI	4385612
BAPTA-AM	Sigma	A1076-25MG
Nifedipine	TOCRIS	600
KN92	TOCRIS	4130
KN93	TOCRIS	1278
MspI	NEB	R0106S
HpaII	NEB	R0171S
Power SYBR Green PCR Master Mix	Applied Biosystems	4367659
Cholera Toxin Subunit B, Alexa Fluor 594 Conjugate	Invitrogen	C22842
Formaldehyde	Sigma	F8775-25ML
Protein G Dynabeads	Life Technologies	10003D
Proteinase K	NEB	P8107S
Critical Commercial Assays		
DIG RNA labeling kit (SP6/T7)	Roche Applied Science	11175025910
Zamboni's fixative	Newcomer Supply	1459
RNA clean and concentrator	Zymo Research	R1017
FISH Tag (alexa fluor 594)	ThermoFisher	F32954
SuperScript III Reverse Transcriptase	Invitrogen	18080093

(*Continued on next page*)

Continued		
REAGENT or RESOURCE	SOURCE	IDENTIFIER
SuperSignal West Dura Extended Duration Substrate	ThermoScientific	34075
pCR 2.1 TOPO Cloning Kit	Invitrogen	K450002
EZ DNA Methylation-Lightning Kit	Zymo Research	D5030
Experimental Models: Organisms/Strains		
Mouse: Adult C57Bl6/J	Charles River	N/A
Mouse: $Tdg^{f/f}$ C57Bl6/J	A.B., unpublished data	N/A
Mouse: Pirt-GCaMP3 C57Bl6/J	Kim et al., 2016	N/A
Mouse: $Pten^{f/f}$ mice C57Bl6/J	Park et al., 2008	N/A
Recombinant DNA		
AAV2/9 virus	Guo et al., 2011b	N/A
AAV2/9 GFP-Cre virus	UPenn Vector Core	V1656
Sequence-Based Reagents		
Control shRNA and shRNAs for mouse Tet1, 2, and 3	Yu et al., 2015	N/A
TDG shRNA AAATGTCAGGAAGAGTCTTGG	This paper	N/A
Digoxigenin-labeled antisense riboprobe: Tet1 (3353–3860 bp), Tet2 (2808–3366 bp), Tet3 (4977–5616 bp)	This paper	N/A
qPCR primers	This paper	See Table S1
Software and Algorithms		
NeuronJ	Erik Meijering	https://imagescience.org/meijering/software/neuronj/
ImageJ	NIH	https://imagej.nih.gov/ij/
QUMA	RIKEN	http://quma.cdb.riken.jp/
Other		
30 gauge syringe	Hamilton	N/A
Ultra-fine hemostatic forceps	F.S.T.	13021-12
Radiant heat light source	IITC	33 Analgesia Meter
Confocal Microscope	Zeiss	800
Applied Biosystems	ThermoFisher	7500
Dumont number 5 forceps	Roboz	RS-5015
Hybond-N+ membrane	GE Healthcare	RPN2020N
UV stratalinker	Stratagene	1800
4-16% Mini-PROTEAN TGX Precast Protein Gels	Bio-rad	4561083
Trans-Blot Turbo Mini PVDF Transfer Packs	Bio-rad	1704156
Trans-Blot Turbo Transfer Starter System	Bio-rad	1704155
Dounce tissue grinder set	Sigma	D9938-1SET
Bioruptor plus	Diagenode	300

CONTACT FOR REAGENT AND RESOURCE SHARING

Further information and requests for resources and reagents should be directed to and will be fulfilled by the Lead Contact Hongjun Song (shongjun@mail.med.upenn.edu). There are no restrictions on any data or materials presented in this paper.

EXPERIMENTAL MODEL AND SUBJECT DETAILS

Animals

All animal procedures used in this study were performed in accordance with the protocol approved by the Institutional Animal Care and Use Committee of Johns Hopkins University School of Medicine and Boston Children's Hospital. Four mouse lines were used for this study: C57Bl6/J mice, a DRG neuron reporter mouse line that expresses GCaMP3 from the endogenous *Pirt* locus (Kim et al., 2016), $TDG^{f/f}$ (to be described in detail elsewhere; A.B., unpublished data), and $Pten^{f/f}$ (Bonaguidi et al., 2011; Park et al., 2008). Adult mice (6-8 weeks) were used. Housing and husbandry conditions followed standard settings within the Miller Research Building

Animal Facilities, as certified by the Animal Care and Use Committee of Johns Hopkins University and were the same for all mouse lines used in this study. No procedures were performed outside of the experiments listed specifically in this study. Experimental and control mice were male littermates housed together before the experiment.

METHOD DETAILS

AAV constructs

Control shRNA and shRNAs for mouse Tet1, Tet2, and Tet3 were previously characterized (Guo et al., 2011c; Yu et al., 2015). Tet3 shRNA efficacy was further validated by Q-PCR in DRG neurons in vitro and in vivo (Figures S2B and 3A). shRNA for mouse TDG contained the following short-hairpin sequence: AAATGTCAGGAAGAGTCTTGG and its efficacy was validated by Q-PCR in DRGs in vivo (Figure S4B). High titers of recombinant AAV2/9 virus transducing shRNA were generated as previously described (Guo et al., 2011c; Song et al., 2012). In addition, the recombinant AAV2/9 vector for Cre was purchased from the UPenn Vector Core.

DRG cultures and neurite outgrowth assay

For cell culture experiments (Figure S2A-E), lumbar DRGs from adult mice were rapidly dissected and digested in a solution of Collagenase II (200 U/mL, Worthington Biochemical Corporation, Lakewood, NJ) and Dispase II (2.5 U/mL, Roche Diagnostics) in HBSS at 37°C for 30 min. Tissues were then mechanically dissociated into cell suspension by gentle trituration with a 1 mL pipette tip. Cell suspension was layered on a BSA cushion (10% w/v in F12/MEM) and centrifuged at 600 g for 15 min to remove myelin and axon debris. Purified neurons were then cultured on laminin-coated coverslips in F12/MEM media complemented with 10% FBS and penicillin-streptomycin at 37°C. Cultures were infected with AAV co-expressing GFP and different shRNAs for 5 days. Cultures were then trypsinized (0.025% Trypsin-EDTA) for 5 min at 37°C, gently triturated in fresh medium with 10% FCS, and cultured for additional 16 hr. Cells were fixed with 4% PFA and neurites were visualized by immunostaining of β-tubulin (Tuj1; Sigma, 1:1000). The percentage of neurons bearing neurites was quantified by counting those with neurites longer than the diameter of its soma. The length of the longest neurite in each cell was measured in neurite-bearing neurons using the NeuronJ software. Approximately 150 cells were scored per condition and three independent sets of experiments were performed.

For the pharmacological experiments (Figure S1D), lumbar vertebrae were rapidly dissected and treated with BAPTA-AM (50 μM), KN92 or KN93 (10 μM) in DMEM/F12 media for 1 hr at 37°C in a humidified atmosphere containing 5% CO_2. Total RNA were then isolated from DRGs using TRIzol and RNA Clean and Concentrator (Zymo Research) for the subsequent Q-PCR assay.

Animal surgery

For intrathecal injection of AAV2/9 viruses, adult mice were anesthetized and shaved to expose the skin around the lumbar region. A total of 3 μL of viral solution was injected to cerebrospinal fluid between vertebrae L5 and L6 using a 30 gauge Hamilton syringe (Figures S1G and S1H). The injection needle was left in place an additional 2 min to allow the fluid to diffuse. Mice were left to recover for 3 weeks to ensure substantial viral expression prior to behavioral or surgical procedures.

For SNL, mice were anesthetized and a small incision was made on the skin at the mid-thigh level. The sciatic nerve was exposed after opening the fascial plane between the gluteus superficialis and biceps femoris muscles. The nerve was carefully freed from surrounding connective tissue and then crushed for 15 s at 3 clicks of ultra-fine hemostatic forceps (F.S.T. 13021-12). The crush site was labeled by stitching a 10-0 nylon suture through the epineurium. Skin was then closed with two suture clips. For the sham surgery, the sciatic nerve in the contralateral side was exposed and mobilized but left uninjured. For the thermal withdrawal test and skin biopsy experiments, the saphenous nerve was ligated and transected above the knee region after sciatic nerve crush, so that the hind paw epidermis can only be innervated by regenerating sciatic nerve axons (Figure S2J).

Behavioral analysis

The thermal withdrawal behavioral test was performed following a previously established protocol (Wright et al., 2014). Briefly, mice were placed on a glass surface with a consistent temperature of 30°C. The plantar surface of hind paw was tested using a focused, radiant heat light source (model 33 Analgesia Meter; IITC/Life Science Instruments, Woodland Hills, CA, USA). A timer linked to the light source was used to measure the paw-withdrawal latency. Only quick hind paw movements away from the stimulus were considered to be a withdrawal response, and seven individual measurements were repeated for each paw.

In situ hybridization

In situ hybridization was performed on PFA-fixed DRG sections (20 μm thickness) as described previously (Jang et al., 2013; Ma et al., 2009). Digoxigenin-labeled antisense riboprobes specific for the coding sequences of mouse Tet1 (3353–3860 bp), Tet2 (2808–3366 bp) and Tet3 (4977–5616 bp) were generated using the DIG RNA labeling kit (Roche Applied Science) according to the manufacturer's instructions. DRG sections were hybridized with riboprobes at 60°C overnight, and then washed once in 5X SSC and three times in 0.2X SSC for 30 min each at 60°C. DRG sections were incubated with alkaline phosphatase-conjugated anti-digoxygenin antibody at 4°C overnight and developed in nitroblue tetrazolium (NBT, 35 μg/ml)/5-bromo-4-chloro-3-indolyl phosphate (BCIP, 18 μg/ml) solution at room temperature to visualize hybridized riboprobes. Experiments for different conditions were processed in parallel for comparison. For the combined immunocytochemistry and fluorescence in situ (Figure 1A), the same in situ procedure was followed

as above with the following exceptions. First, an RNA probe was generated and conjugated to alexa fluor 594 (FISH Tag #F32954). Second, in situ hybridization was followed by immunostaining for GFP (goat anti-GFP Rockland; 1:500), incubated at 4°C overnight and followed by a two-hour room temperature incubation of cy2-conjugated secondary (Jackson ImmunoResearch; 1:500).

Western blot analysis

L4/L5 injured or naive DRGs were rapidly dissected and extracted protein samples were run on 4%–16% Mini-PROTEAN® TGX Precast Protein Gels (Bio-rad) and transferred to PVDF membrane using the transblot turbo system (Biorad) following manufacturer's instructions. The membrane was blocked overnight in 5% dry milk at 4°C with rocking. Anti-Tet3 antibodies (Abiocode; 1:1000) were applied overnight at 4°C followed by HRP-conjugated mouse anti-mouse IgG antibody (Santa Cruz; 1:4000). Protein loading was verified by mouse anti-GAPDH.

Gene expression and methylation analyses

For Q-PCR analysis, L4 and L5 DRGs were rapidly dissected from adult mice and homogenized with Trizol (invitrogen) to extract total RNA. Isolated RNA was reverse transcribed to cDNA (Invitrogen) and the expression level of target genes was measured by Q-PCR with Fast SYBR Green Master Mix (ABI). Specific primers used in this study are listed in Table S1.

A restriction enzyme-based methylation assay was performed to quantify levels of DNA methylation at select loci in mouse DRG DNA as previously described (Guo et al., 2011a, 2014). Briefly, 500 ng of genomic DNA from neuronal nuclei enriched by a sucrose cushion method were digested with MspI, HpaII or mock for 8 hr at 37°C. The reaction was stopped by treatment of proteinase K for 10 min at 40°C and heat-inactivation for 5 min at 95°C. DNA samples were then diluted by ddH_2O to 150 μL final volume and were assayed by Q-PCR (Applied Biosystems 7500) using Power SYBR® Green PCR Master Mix (Applied Biosystems). Primers flanking specific HpaII digestion sites (CCGG) are listed in Table S1.

In vivo DRG axon regeneration assay

Adult mice were anaesthetized and perfused with 4% PFA in PBS. For cross-section analyses, the sciatic nerve was harvested at 7 days after crush when degeneration of pre-existing axons of mature neurons was complete (Di Maio et al., 2011; Shin et al., 2012). DRGs were dissected and post-fixed in fixative at 4°C for 5 min and the sciatic nerve was post-fixed overnight, and then cryoprotected in 30% sucrose (wt/vol) for 24 hr at 4°C. The nerve was sectioned into 10 μm thickness at every 1 mm from 1 mm proximal to injury site (−1) to 6 mm distal to injury site. The sectioned nerves were stained with anti-GFP antibody and the total number of axons was quantified at each distance by using ImageJ software. The section 1 mm proximal to injury site served as control and the axon number in other sections was normalized to the control for each animal to assess the regeneration rate.

For the longitudinal sections assay, sciatic nerves were dissected at SNL D3 and postfixed with 4% PFA. Longitudinal sections were stained with SCG10 (Novus Biologicals, NBP1-49461). SCG10 fluorescence intensity was measured by NIH ImageJ along the distance as previously described (Di Maio et al., 2011; Shin et al., 2012). An SCG10 intensity plot was drawn with average intensities calculated from non-overlapping 10 μm regions and normalized to that observed at the crush site.

Immunohistology

Immunohistology was performed as described previously (Duan et al., 2007). The slides were incubated with primary antibodies at 4°C overnight. Primary antibodies used in this study include: mouse anti-Tuj1 (Sigma; 1:1000 or BioLegend; 1:2000), mouse anti-phospho-c-Jun (Cell Signaling; 1:300), rabbit anti-5hmC (Active Motif; 1:5000), rabbit anti-ATF3 (Santa Cruz; 1:500), rabbit anti-PGP9.5 (AbD Serotec; 1:800), goat anti-GFP (Rockland; 1:500), mouse Anti-NeuN (Millipore; 1:500), mouse anti-Glutamine Synthetase (Santa Cruz sc-74430; 1:300), rabbit anti-SCG10 (Novus Biologicals, NBP1-49461, 1: 2000), and anti-cleaved (active) form of caspase 3 (Invitrogen, 9H19L2; 1:500). Cy2–, Cy3– or Cy5–conjugated secondary antibodies (Jackson ImmunoResearch; 1:500) to appropriate species were incubated at room temperature for 2 hr. The images were acquired by confocal microscopy (Zeiss 710).

Images were analyzed with ImageJ software (National Institutes of Health). Quantification of the proportion of ATF3 or p-c-Jun expressing DRG neurons was determined by counting the number of immunoreactive (with nuclear signal) and non-immunoreactive (without nuclear signal) neurons. The cutoff value for determining the threshold of immunoreactivity was based on the negative cells in naive samples processed in parallel. All cells with fluorescence signal above threshold were considered positive. At least 50 GFP^+ DRG neurons per mouse were counted on randomly chosen sections from L4 and L5 DRGs.

For skin biopsies, glabrous footpad skin from hind paws was harvested by punch biopsy (Figure S2J). The biopsy was immersion-fixed in Zamboni's fixative overnight at 4°C, and cryoprotected in 30% sucrose. The specimens were then sectioned at 20 μm, mounted on gelatin coated slides and stained with rabbit anti-PGP9.5 antibody to visualize nerve fibers. To quantify regenerative nerve fibers, we defined 3 zones based on the structure of skin (Figure 2F). Zone 1 is the dermis layer where the subepidermal nerve plexus length (SNPL) was determined and divided by the length of epidermis. Zone 2 and Zone 3 are defined based on the boundary between stratum granulosum (SG) and stratum spinosum (SS) sub-layers in epidermis (Figure 2F). The density of epidermal nerve fibers was measured by counting numbers of nerve fibers per mm of epidermis. Nerve fibers branching within Zone 3 were counted as one, whereas nerve fibers branching within Zone 2 were counted separately.

Neuronal nuclei isolation

For 5hmC quantification, we enriched DRG neurons with a sucrose cushion method (Kozlenkov et al., 2014). Briefly, frozen DRG tissues were ground into fine powder in a dry ice/ethanol cooling bath and homogenized in 3 mL of hypotonic buffer containing 20 mM Tris-HCl (pH 7.4), 10 mM NaCl, and 3 mM $MgCl_2$. Samples were then suspended in nuclei resuspension buffer containing 3 mM $MgCl_2$, 5 mM $CaCl_2$, 10 mM Tris-HCl (pH7.5), 0.5 mM DTT, 1x proteinase inhibitor (Roche), and 0.32 M sucrose. The crude nuclei were layered onto a sucrose cushion buffer containing 0.5 mM $MgCl_2$, 0.5 mM DTT, 1x proteinase inhibitor, and 0.88 M sucrose, and centrifuged at 2800 g for 15 min at 4°C to enrich the neuronal nuclei population. The neuronal nuclei were then resuspended in nuclei resuspension buffer for cytometry analysis or methylation sensitive Q-PCR analysis.

5hmC dot blot analysis

Dot blot analysis of 5hmC was performed as previously described (Guo et al., 2011c; Yu et al., 2015). Briefly, genomic DNA samples from different treatment groups were adjusted to a concentration of 100 ng/μl, heat-denatured at 95°C for 5 min, and chilled on ice for 1 min. Samples were applied to Hybond-N+ membranes (GE Healthcare), and then cross-linked by a UV stratalinker 1800 (Stratagene). Membranes were blocked by 5% dry milk (wt/vol), and incubated with anti-5hmC antibody (Active Motif; 1:5,000) followed by HRP-conjugated donkey anti-rabbit IgG antibody (Santa Cruz; 1:1000). Signal was visualized by SuperSignal West Pico Chemiluminescent Substrate (Thermoscientific).

Bisulfite sequencing

Bisulfite sequencing analysis was performed as previously described (Ma et al., 2009). Briefly, genomic DNA was bisulfite converted using commercial reagents (Zymo Research). The converted DNA was then used as a template for PCR amplification of regions of interest with specific primers (listed in Table S1). PCR products were gel-purified and cloned into the pCR 2.1 TOPO vector (Invitrogen). Individual clones were sequenced and aligned with the reference genomic sequence.

ChIP analysis

Freshly dissected DRGs were cut into fine pieces and incubated in 1% formaldehyde (Sigma) in Dulbecco's PBS (DPBS) for 15 min at room temperature with continuous rocking. 0.125 M glycine was added to the solution and incubated for 5 min to quench cross-links. After washing twice with ice-cold DPBS, tissue pieces were resuspended in cell lysis buffer (50 mM Tris-HCl pH 8.0, 10 mM EDTA, and 1% SDS), homogenized using a Dounce homogenizer (Kimble Chase) and then incubated on ice for 30 min. The samples were sonicated by a Bioruptor plus (Diagenode) for 25 cycles (30 s on, 30 s off) at the high intensity setting. After centrifugation, the supernatant was diluted 10 times in IP dilution buffer (0.01% SDS, 1.1% Triton X-100, 16.7 mM Tris-HCl pH 8.0, 1.2 mM EDTA, and 167 mM NaCl). Anti-Tet3 (Jin et al., 2016) or rabbit IgG (3 μg; Cell Signaling 2729) antibodies were added and incubated at 4°C overnight. Protein G Dynabeads (Life Technologies) were then added to the samples and incubated at 4°C for 2 hr. The beads were washed twice with low-salt wash buffer (0.1% SDS, 0.1% Triton X-100, 2 mM EDTA, 20 mM Tris pH 8.0, and 150 mM NaCl), twice with high-salt wash buffer (0.1% SDS, 0.1% Triton X-100, 2 mM EDTA, 20 mM Tris pH 8.0, and 500 mM NaCl), twice with IP wash buffer (1% deoxycholic acid, 1% Igepal, 100 mM Tris pH 9.0, and 500 mM LiCl) and twice with TE buffer (10 mM Tris-HCl pH8.0 and 1 mM EDTA). Freshly made elution buffer (1% SDS and 0.1 M $NaHCO_3$, pH 8.0) was added to the beads, and chromatin was eluted at 65°C in a thermomixer for 1 hr. After removing beads, crosslinking was reversed in 0.3 M NaCl solution at 65°C overnight. Proteinase K (NEB) was then added to the decrosslinked chromatin solution and incubated for an additional 2 hr at 55°C. The eluted DNA fragments were extracted using phenol:chloroform:isoamyl alcohol (25:24:1) and precipitated by isopropanol and glycogen. Region-specific primers for Q-PCR are listed in Table S1.

Optic nerve injury and quantification

The procedure was performed as previously described (Park et al., 2008). Briefly, Individual AAV-shRNA for Ctrl, Tet1, Tet2, and Tet3 was mixed with AAV-Cre and intravitreally injected to the left eyes of adult $PTEN^{f/f}$ mice. Two weeks after viral injection, the left optic nerve was exposed intraorbitally and crushed with jeweler's forceps (Dumont number 5; Roboz) for 5 s, approximately 1 mm behind the optic disc. To visualize regenerating axons, RGC axons in the optic nerve were anterogradely labeled by 1 μl of cholera toxin β subunit (CTB; 2 μg/μl; Invitrogen) 12 days after injury. Animals were fixed by 4% PFA 2 days after CTB injection in the eye. Quantification of regenerating axons was also performed according the previously described method (Park et al., 2008). Specifically, for each animal the number of CTB labeled axons was estimated by counting the number of CTB-labeled fibers extending different distances from the end of the crush site in 5 sections (every 4^{th} section) per animal. The cross-sectional width of the nerve was measured at the point at which the counts were taken and was used to calculate the number of axons/mm of nerve width. The number of axons/mm was then averaged over all sections. Σad, the total number of axons extending distance d in a nerve having a radius of r, was estimated by summing over all sections having a thickness t (8 μm): $\Sigma ad = \pi r2 \times [\text{average axons/mm}]/t$.

QUANTIFICATION AND STATISTICAL ANALYSIS

The studies were not blind in data collection. Data in figure panels reflect several independent experiments performed on different days. The number of experiments for each experimental group is indicated in the figure legends. No data was excluded. For some

quantification, data was normalized as indicated in figure legends. An estimate of variation within each group of data is indicated using standard error of the mean (SEM). We performed two-way ANOVA tests for assessing the significance of differences between two treatments (See each figure for details). For comparing numbers of methylated and unmethylated cytosines from different conditions, Fisher's exact tests were performed.

DATA AND SOFTWARE AVAILABILITY

See the Key Resources Table.

Neuron, Volume *94*

Supplemental Information

An Intrinsic Epigenetic Barrier for Functional Axon Regeneration

Yi-Lan Weng, Ran An, Jessica Cassin, Jessica Joseph, Ruifa Mi, Chen Wang, Chun Zhong, Seung-Gi Jin, Gerd P. Pfeifer, Alfonso Bellacosa, Xinzhong Dong, Ahmet Hoke, Zhigang He, Hongjun Song, and Guo-li Ming

Supplementary Figures

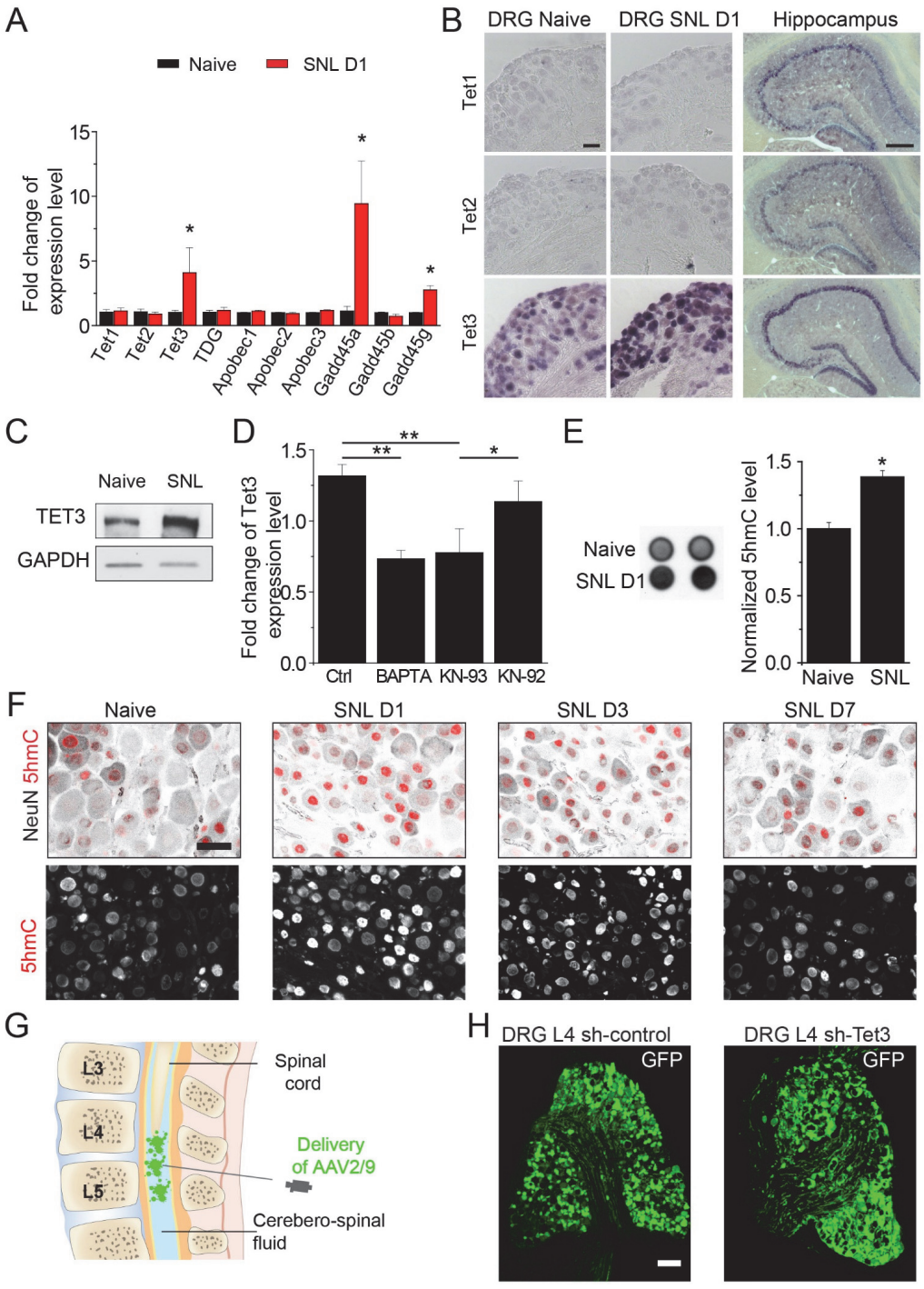

Figure S1. SNL up-regulates Tet3 and 5hmC levels in adult DRG neurons in vivo, related to Figure 1.

(**A**) Expression profiling of DNA demethylation mediators in both naïve and axotomized L4 DRG of adult mice. The mRNA expression level was assessed by Q-PCR at SNL D1. Values represent mean ± SEM (n = 3; **P* < 0.05; two-way ANOVA).

(**B**) *In situ* hybridization of Tet1, Tet2 and Tet3 in naïve and SNL D1 DRGs and in the adult mouse hippocampus (as a positive control). Scale bars: 50 μm.
(**C**) Sample western blot image of Tet3 expression levels in DRGs under the naïve condition and at SNL D1.
(**D**) Signaling mechanism underlying injury-induced Tet3 induction. Adult DRGs were removed from the animals and treated with different pharmacological agents, BAPTA-AM (50 μM), KN92 or KN93 (10 μM) for 1 hr, followed by analysis of Tet3 expression by Q-PCR. Values represent mean ± SEM (n = 4-6 each; ** P <0.01; *P < 0.05; ANOVA).
(**E**) Dot blot analysis of 5hmC levels in DRGs at SNL D1. Neuronal nuclei were enriched from naïve and axotomized DRGs via the sucrose cushion method followed by genomic DNA extraction. 100 ng DNA was spotted onto nitrocellulose membrane and 5hmC levels were detected with anti-5hmC antibody. Shown are sample images and quantification of the signal density. Values represent mean ± SEM (n = 3; *P < 0.05; two-way ANOVA).
(**F**) Sample images of immunostaining of 5hmC and NeuN before and at different time points after SNL. Scale bar: 50 μm. See quantifications in **Figure 1D**.
(**G**) A schematic diagram illustrating intrathecal injection of AAV to infect L4/5DRG neurons in adult mice in vivo.
(**H**) Sample images of GFP-labeled neurons in DRGs at three weeks after AAV2/9 injection to express GFP together with either control shRNA or Tet3 shRNA. Scale bar: 50 μm.

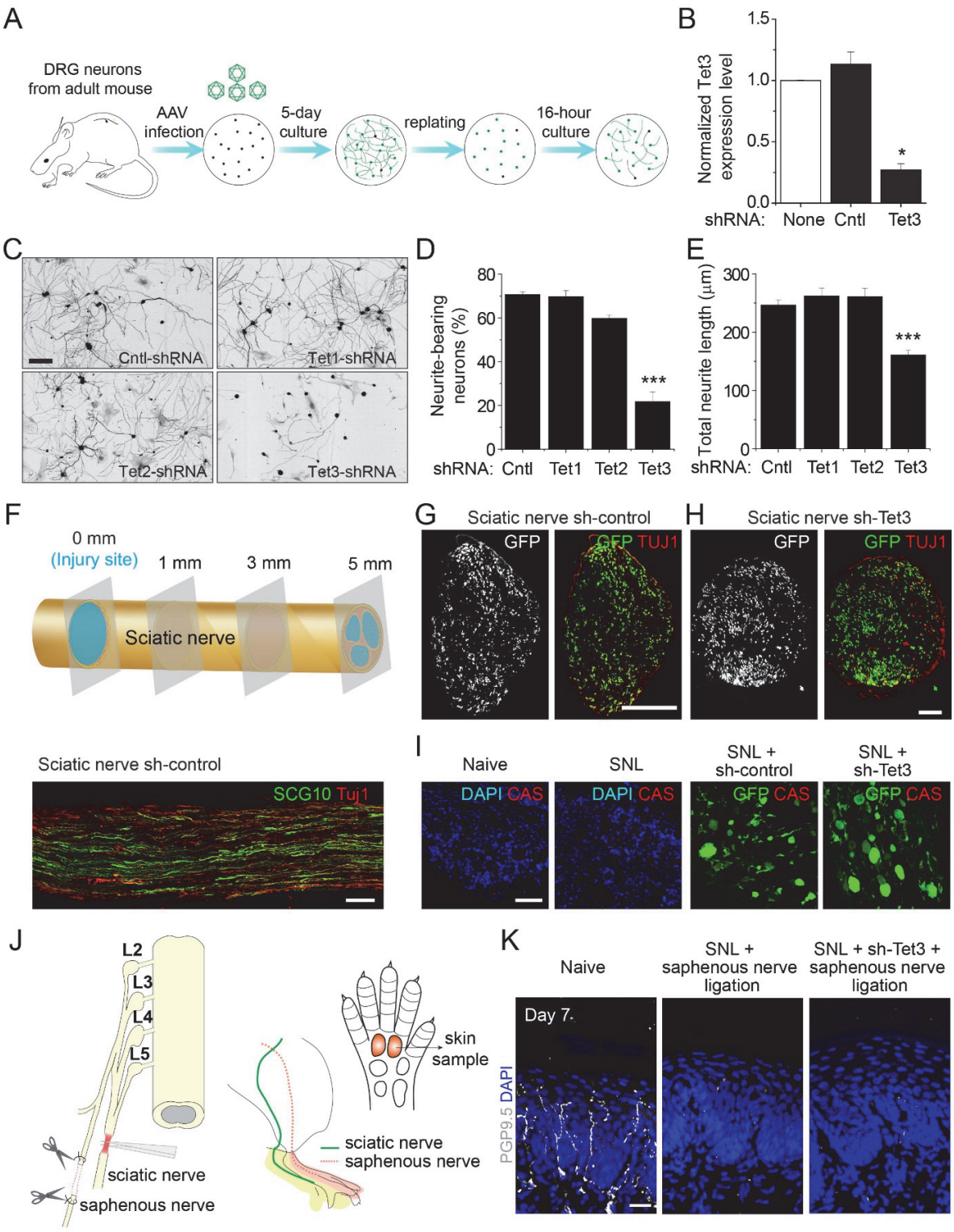

Figure S2. Tet3 is required for robust axon regeneration of adult DRG neurons, related to Figure 2.

(**A-E**) In vitro neurite outgrowth assay. Shown in (**A**) is a schematic diagram illustrating the DRG neuron re-plating assay for neurite outgrowth. Shown in (**B**) is quantification of the efficacy of Tet3 shRNA in vitro. Values represent mean ± SEM (n = 3; **P* < 0.05; two-way ANOVA). Also shown are

sample images (**C**; scale bar: 100 μm) and quantification of percentages of neurite bearing neurons (**D**) and total neurite length (**E**). Values represent mean ± SEM (n = 3 independent experiments; ***$P < 0.001$; two-way ANOVA).

(**F-I**) A schematic diagram of quantification of regenerating axons in the sciatic nerve at distal distances from the injury site (set as 0 mm; **F**). The bottom panel shows a sample image of $SCG10^+Tuj1^+$ regenerating axons (Scale bar: 20 μm). Also shown are sample images of cross sections of sciatic nerve at three weeks after AAV2/9 injection to express GFP together with either control shRNA (**G**) or Tet3 shRNA (**H**) in the absence of SNL (Scale bars: 50 μm). Immunostaining of cleaved caspase 3 (CAS) showed little death of DRG neurons under different conditions (**I**; scale bar: 50 μm).

(**J**) Schematic diagrams of skin re-innervation assay. Shown in the left panel is a schematic illustration of SNL and saphenous nerve ligation. Shown in the middle panel is a diagram of foot innervation illustrating the major innervation of mouse hind paw by both sciatic and saphenous nerves. Shown in the right panel are the glabrous footpad regions for skin biopsy.

(**K**) Sample images of skin nerve fibers from naïve animals, animals 7 days after SNL and saphenous nerve ligation, and Tet3-shRNA infected animals 7 days after SNL and saphenous nerve ligation. Note that the SNL and saphenous nerve ligation resulted in complete denervation of GFP^+ axons in the footpad skin at D7 after injury for both control and Tet3 KD animals. Scale bar: 20 μm.

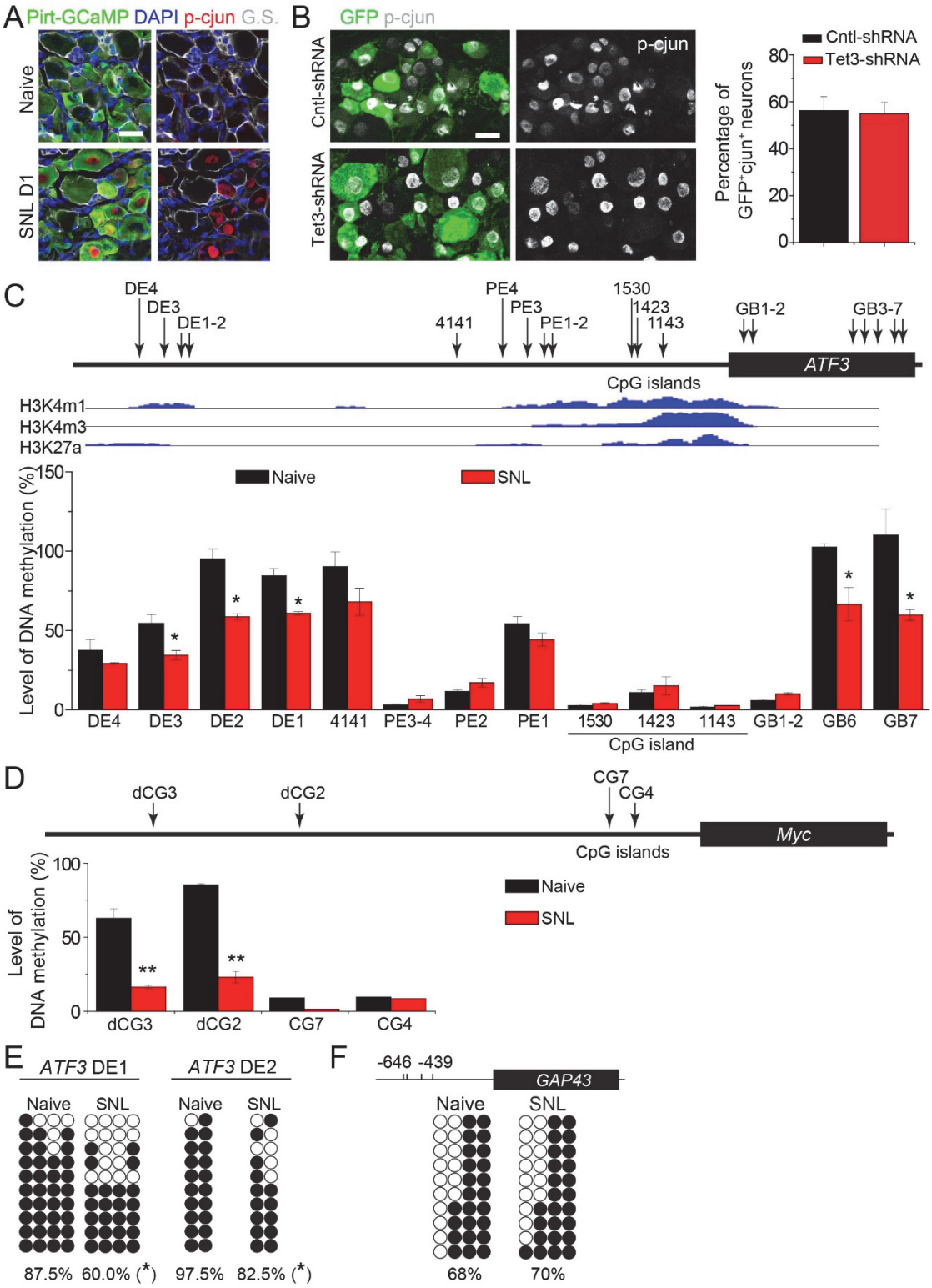

Figure S3. Changes of DNA methylation levels on certain RAGs before and after SNL, related to Figure 3.

(**A-B**) Sample images of immunostaining of phospho-c-Jun (p-cjun), GFP, Glutamine Synthetase (G.S.) in Pirt-GCaMP3 neuronal reporter mice (**A**), and GFP and p-jun in AAV-Ctrl and Tet3 shRNA

treated DRGs (**B**). Scale bars: 20 μm. The percentage of GFP^+ neurons with expression of p-cjun was quantified at SNL D7. Values represent mean ± SEM (n = 3; $P > 0.1$; two-way ANOVA).
(**C**) DNA methylation analysis of the *ATF3* genomic loci. Shown in the top panel is a schematic diagram illustrating the genomic region of *ATF3* gene subjected to analysis. Shown in the middle panel is ChIP-seq data on three histone marks from ENCODE to identify genomic features of different genomic regions (DE: putative distal enhancer; PE: proximal enhancer; 4141: 4141 bp prior to ORF; GB: gene body; ENCODE-LICR-Histone Track, UCSC Genome Informatics). Shown in the bottom panel is a summary of DNA methylation levels at specific regions. Nuclei harvested from naïve or SNL D1 DRGs were subjected to a sucrose cushion to partially enrich neuronal nuclei. Genomic DNA was then digested with either methylation-sensitive (HpaII) or insensitive enzymes (MspI). Primers spanning specific CCGG sites were used to amplify several putative regulatory regions of *ATF3*. Values represent mean ± SEM (n = 3; $*P < 0.05$; two-way ANOVA).
(**D**) DNA methylation analysis of the *c-Myc* genomic loci, similar to (**C**). Values represent mean ± SEM (n = 3; $**P < 0.01$; two-way ANOVA).
(**E-F**) Bisulfite sequencing analysis of *ATF3* (**E**) and *GAP43* loci (**F**) in naïve DRG neurons and at SNL D1. $NeuN^+$ neuronal nuclei from L4 and L5 DRGs were purified by FACS. Results for a 200–300 bp region are shown. Each row represents one sequence read and each column represents an individual CpG site within the analyzed region. Filled (black) or open (white) dots represent methylated or unmethylated CpG sites, respectively. Numbers indicate the mean frequency of methylation at all CpG sites examined ($*P < 0.05$; Fisher's exact test).

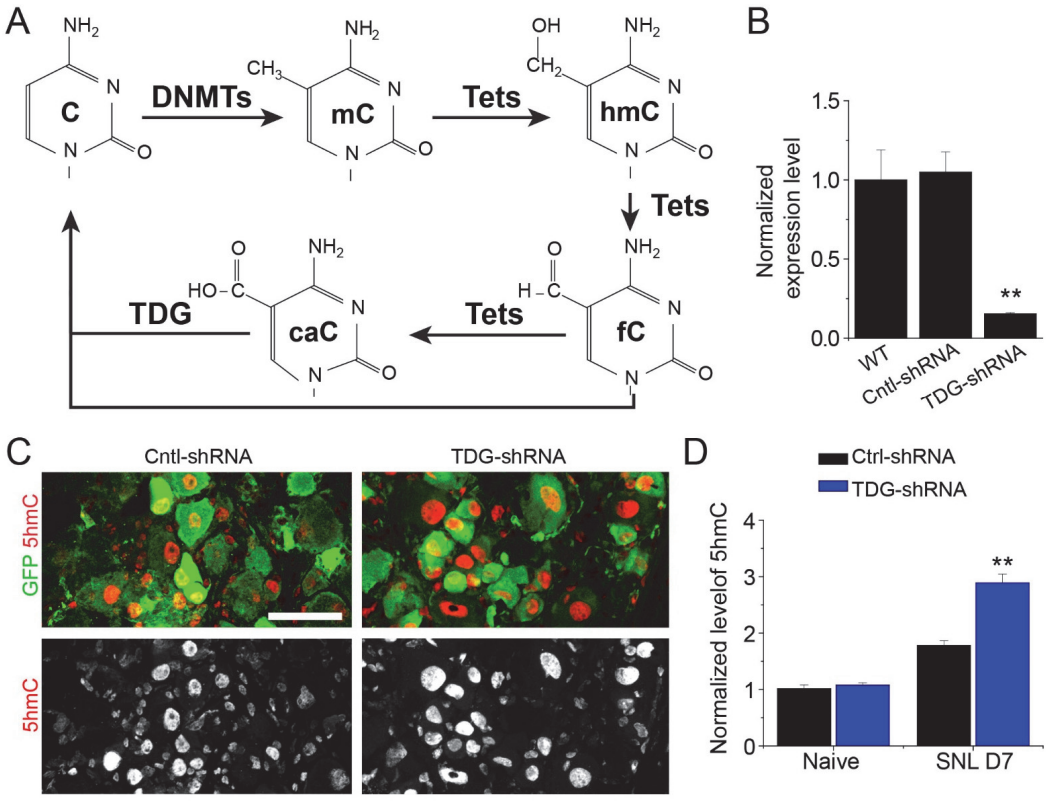

Figure S4. 5hmC level changes in TDG KD DRG neurons after SNL, related to Figure 4.
(**A**) A schematic diagram illustrating known molecular mediators of active DNA demethylation.
(**B**) In vivo knockdown efficacy of TDG shRNA. Adult DRGs were infected with AAV-TDG shRNA or control (Ctrl) shRNA via intrathecal injection. TDG expression was analyzed 21 days later by Q-PCR. Values represent mean ± SEM (n = 3; $^{**}P < 0.01$; two-way ANOVA).
(**C-D**) Immunohistochemical analysis of 5hmC levels in Ctrl and TDG KD DRG neurons of naïve and SNL D7 animals. Same as in **Figure S1E**, shown are sample images (**C**; scale bar: 20 μm) and quantification (**D**). Values represent mean ± SEM (n = 3; $^{**}P < 0.01$; two-way ANOVA).

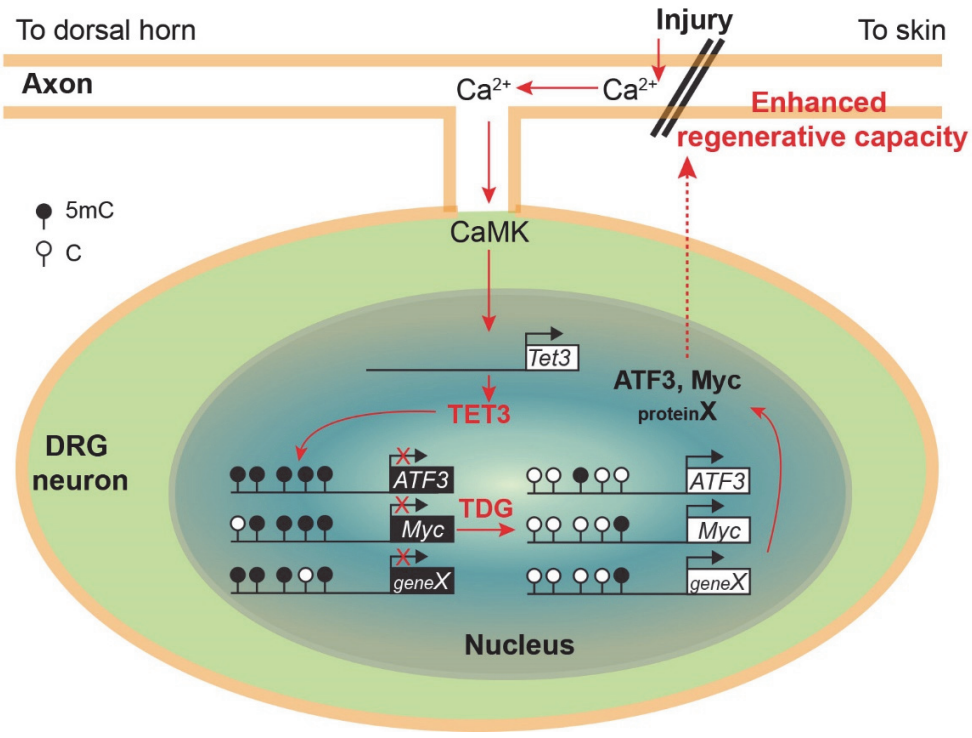

Figure S5. A summary model, related to all Figures.
Peripheral injury of DRG axons leads to calcium influx and calcium waves are back propagated to cell body, where they activate CaMKII, resulting in transcriptional activation of Tet3 in the nuclei. Tet3 is targeted to specific 5mCs of some regeneration-associated genes (e.g. ATF3 and c-Myc) to oxidize them into 5hmCs, which are then converted to Cs via TDG-dependent base excision repair. Demethylation of enhancers and promoters of these genes leads to their expression, which in turn promotes axon growth capacity of adult DRG neurons.

Table S1. List of primer sequences used in the current study, related to Figures 1, 2, 3, 4, S1, S2, S3 and S4.

Primers for Q-PCR analysis of epigenetic regulators	
GAPDH_F	AAGAAGGTGGTGAAGCAGGCATCT
GAPDH_R	ACCCTGTTGCTGTAGCCGTATTCA
Tet1_F	GAGCCTGTTCCTCGATGTGG
Tet1_R	CAAACCCACCTGAGGCTGTT
Tet2_F	TGTTGTTGTCAGGGTGAGAATC
Tet2_R	TCTTGCTTCTGGCAAACTTACA
Tet3_F	CCGGATTGAGAAGGTCATCTAC
Tet3_R	AAGATAACAATCACGGCGTTCT
TDG_F	CCATGTAATGGGGAACCTTG
TDG_R	AAGGGATCTGCTCTGCAAAC
Gadd45a_F	TGAGCTGCTGCTACTGGAGAACGAC
Gadd45a_R	TCCTTCCATTGTGATGAATGTGGGT
Gadd45b_F	GCCCGAGACCTGCACTGCCT
Gadd45b_R	CCATTGGTTATTGCCTCTGCTCTCTT
Gadd45g_F	GGAGACCTGCATTGCATCCTCATTT
Gadd45g_R	ACTCGGGAAGGGTGATGCTGG
Apobec1_F	TCAGGGACCTTATTAGCAGCGG
Apobec1_R	GCCAATAAGCTTCGTTTGAAGGG
Apobec2_F	GACAATGGTGGCAGGCGATTCA
Apobec2_R	GCAGAGATGCTTGACTCGTTGG
Apobec3_F	TGCTACTACCACCGCATGAA
Apobec3_R	CAGCTCCATGGACCGAATCT

Primers for Q-PCR analysis of regeneration associated genes	
Smad1_F	ACTGGCGCAGTCTGTGAAC
Smad1_R	GGTATTCGGCTCCCCAAC
Stat3_F	CTGAGCCCTCAGCAGGAG
Stat3_R	AGGTAGCACACTCCGAGGTC
EGR1_F	GAGCGAACAACCCTATGAGC
EGR1_R	AGGCCACTGACTAGGCTGAA
ATF3_F	AATTGCTGCTGCCAAGTGTC
ATF3_R	CTTCAGCTCAGCATTCACACTC

Primers for enzyme-based methylation Q-PCR	
ATF3_DE1_F	ACAACGAGAAGCCAGCATAG
ATF3_DE1_R	AAGGTACCATCCCCAGTCAG
ATF3_DE2_F	GTCCTTCCCTGTTGATCCAG
ATF3_DE2_R	GAAAGAGAGCCCAGATCCAG
ATF3_DE3_F	TCTGCATTGGCTCCTTACAC
ATF3_DE3_R	TGACTCAGGTGGAACACTGG
ATF3_DE4_F	TGGTTGTACCCTGTCCTTCC
ATF3_DE4_R	TGGAGAAGTTGGGGTGTCTG
ATF3_4141_F	GGCGGTGCCTTTATGACTTA
ATF3_4141_R	TGAGATGAGGTCAGGGAAGC

ATF3_PE1_F	TTGCCACTGTTATCCAGCAC
ATF3_PE1_R	AGTGACAGCTGCAACAGGAG
ATF3_PE2_F	GTCAAGACCCCTGCACAGAC
ATF3_PE2_R	CGATCCCTTCCACATTCCTC
ATF3_PE3-4_F	TCCTTTGGTACATGCCTCAG
ATF3_PE3-4_R	GTTCTGGGGTTTTTCTCCAG
ATF3_GB6_F	CTAGAATCCCAGCAGCCAAG
ATF3_GB6_R	GGCCAGCTAGGTCATCTGAG
ATF3_GB7_F	CAGAGCCTGGTGTTGTGCTA
ATF3_GB7_R	GGTGTCGTCCATCCTCTGTT
ATF3_1530_F	CTGCCTTGGACTTGAGGAAC
ATF3_1530_R	TACGGTCCTGAGGAAAGGTC
ATF3_1423_F	CTTGATTTTGCCCGAAATGT
ATF3_1423_R	GCTGCCTCCATAGCACCTAC
ATF3_1143_F	CAGACCCTCGGAATTACTGG
ATF3_1143_R	CACCGAGCCCTCTTGTACTC
Myc_dCG2_F	TGTGGCTTTCCTGTCCTTTT
Myc_dCG2_R	TAGCGGAATAGCCTGTGGTT
Myc_dCG3_F	GCTGGTGGCTACAAAGGAGA
Myc_dCG3_R	CCAAGAACCTACATTGCCTGT

Primers for bisulfite sequencing

ATF3 BS_DE1_F	GATTAATAGGGAAGGATTAGGGTAAG
ATF3 BS_DE1_R	AAACCAACCTAAATAAATTCCAAAC
ATF3 BS_DE2_F	CCTAAAATACAAAAACCTAAATCAAC
ATF3 BS_DE2_R	GTTTATTAGAAAGTGGGATAGTATAAGTG
NPY BS_F	AGGAAGGTTTTATTAGTAGA
NPY BS-R	AAA AAAACCTACAACCTCCA
GAP43_BS_F	GTGTGTAGTTAGGTTATATA
GAP43_BS_R	CTCATAAATATTTAAACACCTCC
Myc_BS_F	GATGTTATTAGGTTGGGGTATAGT
Myc_BS_R	ACAATAAATAAAACTAACCCTCAAAAAATC

Primers for ChIP-Q-PCR

GAP43_CHIP_F	TGAACCTCCATGATTATCAACTG
GAP43_CHIP_R	CTTTCCCAGTACCACAAGAAGG
ATF3_CHIP_DE1_F	ACAACGAGAAGCCAGCATAG
ATF3_CHIP_DE1_R	AAGGTACCATCCCCAGTCAG
ATF3_CHIP_DE2_F	GTCCTTCCCTGTTGATCCAG
ATF3_CHIP_DE2_R	GAAAGAGAGCCCAGATCCAG
ATF3_CHIP_DE3_F	TCTGCATTGGCTCCTTACAC
ATF3_CHIP_DE3_R	TGACTCAGGTGGAACACTGG
Myc_CHIP_dCG2_F	TGTGGCTTTCCTGTCCTTTT
Myc_CHIP_dCG2_R	TAGCGGAATAGCCTGTGGTT